

Final report

1. Project details

Project title	COBRADrive
File no.	64018-0118
Name of the funding scheme	Energiteknologisk Udviklings- og Demonstrations Program (EUDP)
Project managing company / institution	Advent Technologies A/S (Formerly Serenergy A/S)
CVR number (central business register)	29616647
Project partners	-Blue World Technologies (Formerly Danish Power Systems) -Danmark Tekniske Universitet (DTU) -Aalborg Universitet (AAU)
Submission date	29 August 2022

2. Summary

- *English version*

The objective of COBRA Drive was to advance the Reformed Methanol Fuel cell technology to a level where it is capable of replacing traditional diesel engines in Light Commercial Vehicles.

The project ensured development of the technology to a technology readiness level (TRL) where it can be introduced on a commercial basis on early mobility markets. The project focused on the core elements of the Fuel cell stack; membrane electrode assembly (MEA) and flow plates.

The project achieved several of the initial objectives and successfully managed to make several components and systems more effective, from a functional, cost and durability point-of-view; thus increasing TRL and market readiness level.

- *Danish version*

Målet med COBRA Drive var at fremme den reformerede methanol-brændselscelleteknologi til et niveau, hvor den er i stand til at erstatte traditionelle dieselmotorer i lette kommercielle køretøjer.

Projektet sikrede udvikling af teknologien til et teknologisk parathedsniveau (TRL), hvor den kan introduceres kommercielt til mobilitetsmarkeder. Projektet fokuserede på kerneelementerne i brændselscellestakken; membrane electrode assembly (MEA) og flow plader.

Projektet opnåede flere af de oprindelige mål og lykkedes med at gøre flere komponenter og systemer mere effektive, i et funktionalitets-, kost- og holdbarhedsperspektiv og dermed øge TRL og markedsparathedsniveau.

3. Project objectives

- *What was the objective of the project?*

In order to achieve the project objectives of successfully demonstrating the developed products and technological solutions; the work was divided into several work packages, in each of which, the project has demonstrated the advances made throughout the project period. The work package structure was set up as follows:

- WP1 – Project Management
- WP2 – Development of electrode and membrane
- WP3 – Stack and flow plate materials development
- WP4 – RMFC Core optimization
- WP5 – System optimization
- WP6 – System reliability
- WP7 – System performance
- WP8 – Box development and build
- WP9 – Box concept controls
- WP10 – Commercial compliance
- WP11 – Dissemination

In the following, some of the main aspects of the work packages will be highlighted and summarized. WP1 has mainly acted on an operational level in structuring and organizing the project, hence it is not mentioned in the following summary.

Work package 2: Development of electrode and membrane.

<2% catalyst powder waste from delivery to QC approved electrode, deducting recycle catalyst powder at a value of 60% (98% reclaim of metal value).

The catalyst loading resulted from the E300 electrode coating resulted in an average load of 0.87mgPt/cm². Despite achieving the targeted load, the electrode yield was of 75 % in 2017¹. The low electrode yield is caused by the large number of defects and damages caused unintentionally in the downstream processes (i.e., catalyst ink coating, roll winding and unwinding, cutting electrodes in sheets, heat-treatment and final stamping). The different sources of waste are divided in three types. a) process waste, b) geometrical loss and c) quality control waste.

Process waste is related to the catalyst loss (powder) into a liquid catalyst ink and ink losses in the equipment needed to transfer the catalyst ink into the coating machine making use of tubing, pipes, pumps and ink delivery system. The geometrical waste is related to the handling process of the electrode and how the electrodes area stamped and obtained from the electrode belt. Lastly the electrode coating undergoes an inline quality control (QC), therefore the QC waste is the scrap material derived from insufficient electrode loading, uniformity, coating defect and scratches and defect provoked during handling. As a basis for comparison, the varies type of waste source was analyzed in 2017.

¹ Electrode yield is defined as the amount (%) of usable electrode to be used into MEAs.

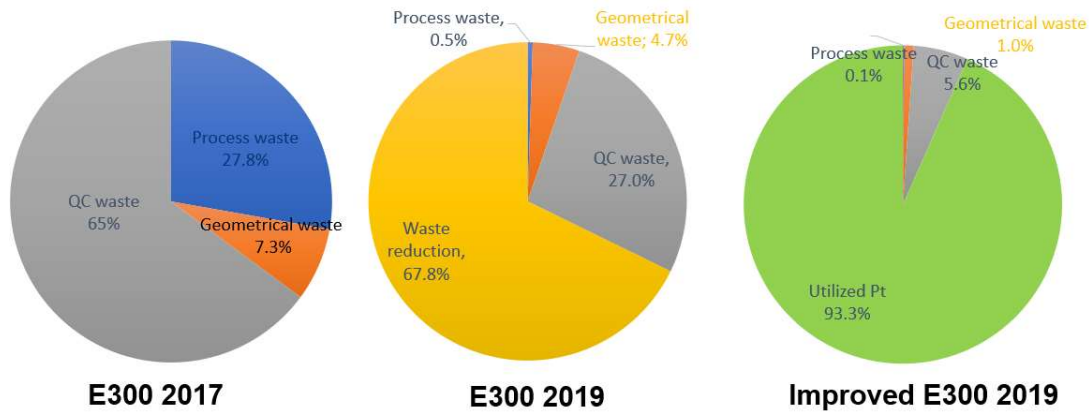


Figure 1. Pie chart on the waste analysis throughout the first part of the project period.

As seen in Figure 1 the largest improvement has been on the process and QC waste showing a reduction of 27,8 to 0,1 % and 65 to 5.6 %, respectively. The geometrical waste improved but to a lower extent, going from 7.3% to 1.0 during the progress made from 2017- 2019-2020. The catalyst ink development has been accompanied by a better knowledge on the process conditions (i.e., slot die coating, handling and storage) over the last project period. Continuous knowledge has been gained on understanding under which conditions the catalyst layers might get damaged. As a result of these know-how has been reduced which implies a significant improvement in the catalyst power utilization, raised from 75 % in 2017 to 93 % in 2019 (See Figure 2).

Gained knowledge has resulted the mitigation of the problems frequently observed during the process development in terms of avoidance of particle agglomerated, edge defects. In addition, new developed inks with better stability as well as the introduction of new homogenization techniques/procedures for particle size evaluation.

The next step in the process development process was to scale up the new ink size recipe meant for longer coating runs. The coating process was outsourced from a third-party facility in Sweden. Corona Covid-19 changed the situation making impossible to travel in/out Denmark. A solution was found where the third party carried out the coatings with remote - video guidance from Blue World, however the technology transfer (i.e., new ink preparation, safety, coating process) took a long time to come to the same level and quality as we could do ourselves.

Due to these constrictions and long lead time of the new materials it was decided to continue to improve the coating production based on the E300 type while working on the technology transfer for the newest ink recipes. For the standard E300 electrode, 72 coatings showed the targeted Pt load (mg/cm²) interval. This is measured by establishing the correlation between the theoretical length to be achieved using a given amount of catalyst compared to the resulting length after the coating proves. All trials were in between the max and min Pt load acceptance level with an improvement in this deviation, from 96 to 99 %.

One of the keys to a uniform MEA performance is a low variation in Pt loading from electrode-to-electrode batch, and with the same ink recipe hitting the same coated length every time is a challenge.

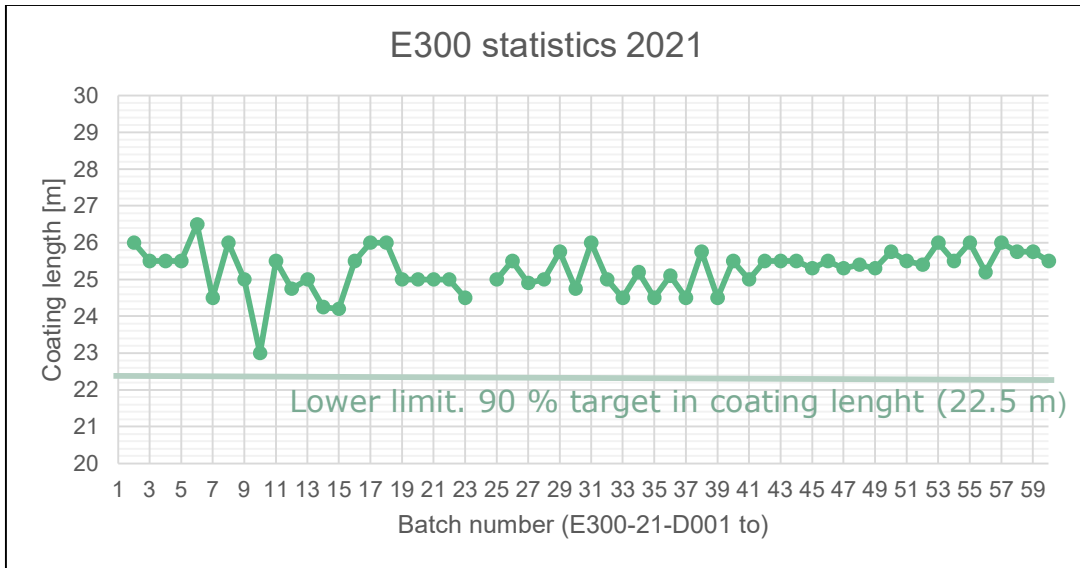


Figure 2. Measured coating length for each E300 coating run for the first 59 batches carried out in 2021.

For E300 electrodes the process waste and QC waste was very high in 2017. However, the different source of material waste has been reduced due to varies improvements in the manufacturing process, such as coating optimization and better electrode handling during electrode curing and stamping into the final electrode size for MEA fabrication.

The distribution of the different source of electrode waste is presented for the period 2017 to 2020. The quality control (QC) and process waste have been greatly reduced whereas the geometrical loss remained unchanged in this period.

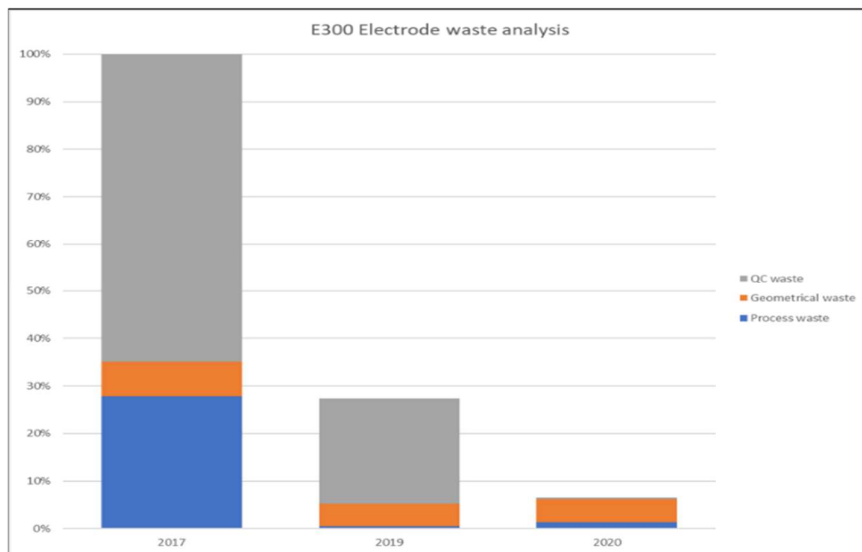


Figure 3 . Electrode waste stream analysis 2017 – 2020.

Having into account all the waste collected from varies sources, the Pt utilization is calculated and presented in Table 1. This is defined as the amount raw catalyst material that it is finally incorporated into the functional electrode as part of the MEA product. As seen, the Pt utilization has been remarkably improved from 2017 to 2020, from 58.4% to 97.5 %.

Table 1. Overview of the electrode waste over the last 5 years

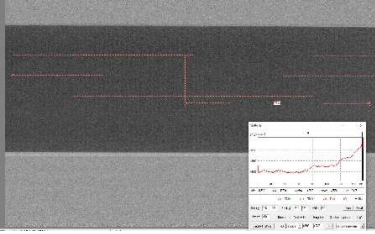
Electrode type	2017	2019	2020	2021	2022
E300	58,4%	89,6%	97,5 %	Stopped	Stopped
E310	Development phase	Development phase	Lab to production	90%	97,5%

During the last quarter of 2021, the machinery and coating machines required for the upscaling of membrane and electrodes were installed. Re-iteration on the process parameters had to be made and ink rheology had to be made due to the different orientation and design of the slot die, as well as the thickness and the coating gap. Due to the characteristics of the new industrial coating machine, the process waste increased in 2021 (e.g., due to larger dead volume in the slot die head and due to larger pump reservoir systems, the ink loss is higher). To our advantage, the quality control waste is reduced due to the improvements made at the ink and process development level). As of 2022, the electrode waste reached again ca. 98 %. The reason for such an improvement is the continuous upscaling of the coating length. The longer the coatings are, the lower waste (process and geometrical) are obtained.

Table 2 (a) shows a series of electrode coating tests carried out at BWT facilities and b) in-line quality control via X-RAY analysis whereby the average Pt load and deviation can be determined and allows for a rapid in-line screening of the coated material as well as the early detection, thereby is possible to correct the process parameters (i.e., velocity, ink flow) whilst running the coating continuously.

Table 2. Pre-series casting trials for anode type E111 – and cathode E310 – C. right X-RAY machine imaging for Pt load verification.

Run no.	Type	Run no.	Type	Run no.	Type
LEC-030	E310 - C	LEC-051	E310 - C	LEC-069	E310 - C
LEC-031	E111 - A	LEC-052	E310 - C	LEC-070	E310 - C
LEC-032	E310 - C	LEC-053	E111 - A	LEC-075	E310 - C
LEC-033	E111 - A	LEC-057	E111 - A	LEC-076	E310 - C
LEC-034	E310 - C	LEC-058	E111 - A	LEC-077	E111 -A
LEC-035	E310 - C	LEC-059	E310 - C	LEC-078	E111 - A
LEC-036	E310 - C	LEC-060	E310 - C	LEC-079	E310 - C
LEC-037	E310 - C	LEC-061	E111 - A	LEC-080	E310 - C
LEC-038	E111 - A	LEC-064	E111 - A	LEC-081	E310 - C
LEC-039	E111 - A	LEC-065	E111 - A	LEC-082	E310 - C
LEC-040	E111 - A	LEC-066	E111 - A	LEC-083	E111 -C
LEC-041	E310 - C	LEC-067	E111 - A		
LEC-048	E310 - C	LEC-068	E111 -A		
LEC-049	E310 - C				
LEC-050	E310 - C				



As a result of the iteration process the Pt loading target is reached. Figure 4 and 5 shows the results of a coating trial before and after the improvements. As seen in Figure 4 , the amount of wasted material during the coating start and stop (beginning and end of the coating process) is extended over a greater length compared to the improved coating run shown in Figure 5. It can also be observed that after the coating process reaches steady state operation, the Pt loading standard deviation falls in the range of 5 – 12 % whereas the standard deviation achieved with the new improved process is systematically below 4%.

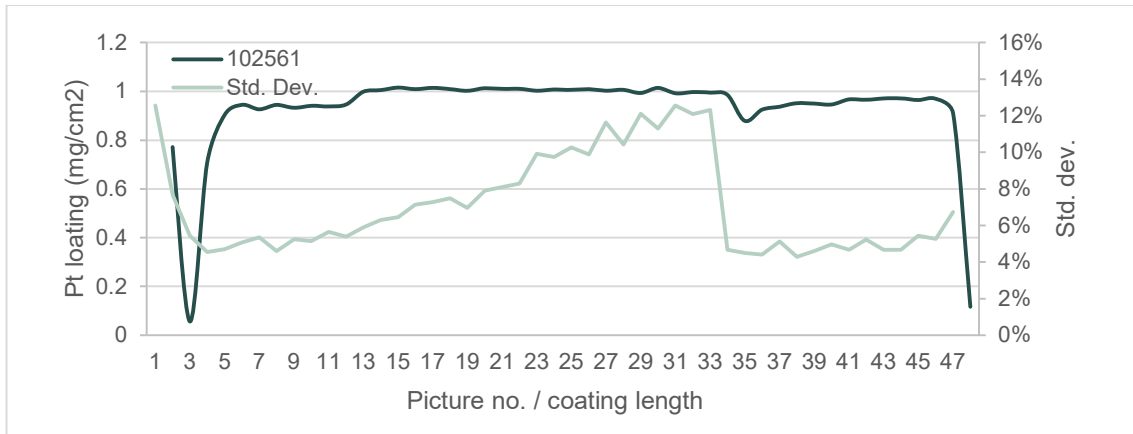


Figure 4. electrode quality control analysts on 310 electrode type (before improvements). Blue line; Pt loading values and Orange; standard deviation for each sample. Sample size of ca. 1 meter. 50 meters

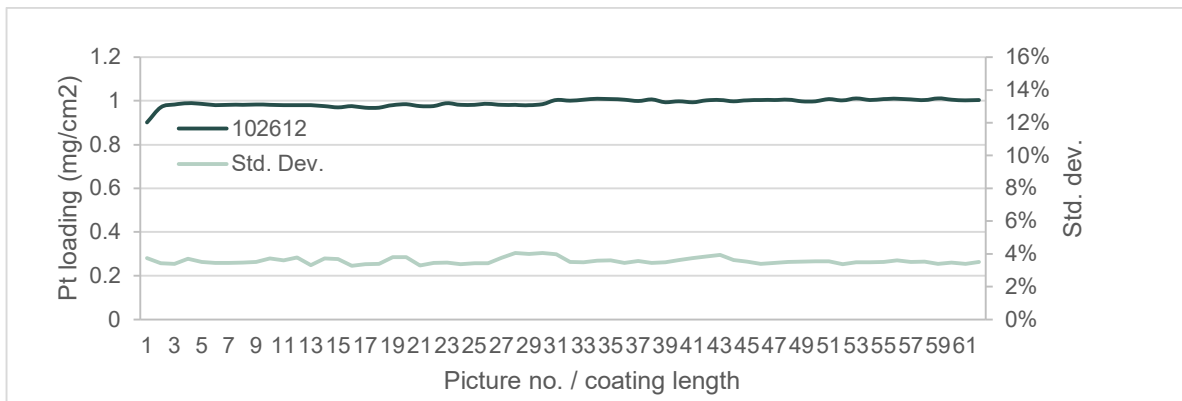


Figure 5. electrode quality control analysis on 310 electrode type (after improvement). Blue line; Pt loading values and Orange; standard deviation for each sample. Sample size of ca. 1 meter. 50meter

The process and quality control waste has been reduced to a large extent, whereas optimization on the geometrical loss is not yet initiated. Alternative to MEA geometrical design (i.e., from round to square corners) and optimization of the overcoating width with respect to the MEA are identified to achieve lower geometrical waste, yet not implemented on production. Upscaling the electrode production in the range of 100 m (done) to 200 m will result in less electrode waste below 2 %

Conclusion: Despite the initial large electrode waste with BWT owned coating machines the electrode waste was reduced to ca. 2%. Process and quality control waste are significantly reduced on (E310 electrode) reaching similar electrode waste for 100 meters coating runs.

<2% PBI waste from QC approved raw material to QC approved membrane for MEA assembly, no deductions of recycle material

The identification of the varies sources of waste for the PBI material is analyzed and divided into the process, geometrical and QC waste. In 2017 the varies waste were 42,2 – 15,1 and 42,7 %, respectively. The analysis showed that the two biggest contributors to the PBI waste where process waste and QC waste.

The process waste came primarily from a multi-layer coating process, some of the material was not usable due to unevenness, bubbles etc. The QC waste came mainly from bubbles, particles and from wrinkles during winding up the finished membrane. (See Figure 6)

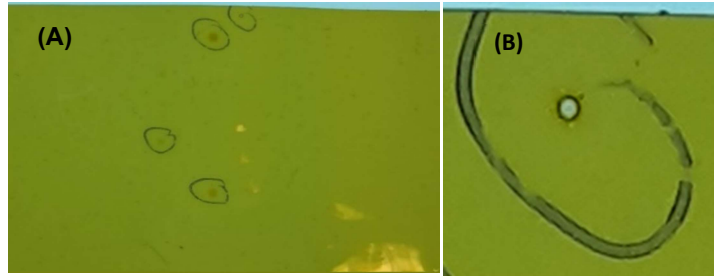


Figure 6. Description of membrane defects observed during quality control. (B) Zoomed Bubbles formed during casting of the membrane and zoomed image of

To reduce the process waste, a number of experiments were conducted to find the optimal operating conditions for the coating, so it was possible to set these before starting the coating instead of adjusting the parameters during the first 1-5 meters of the coating. This has resulted in a reduction of the extra length that had to be coated to reduce the amount of unusable coated PBI material below 1 m.

The geometrical waste is due to 2 cm unusable area at the edges of the membrane due to a drying effect. After several iteration on the drying process the bends disappeared, allowing for additional geometrical waste reduction. This is shown in Figure 7 with a comparison of the geometrical defects in 7.a and the absence of defect in 7.b

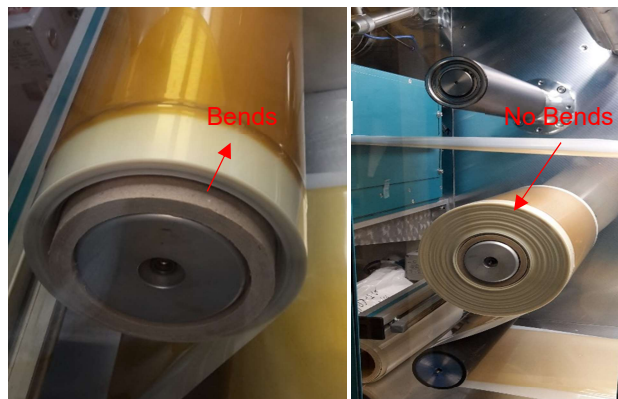


Figure 7: a) Membrane drying edge effect giving a geometrical waste of 1 cm in each side. b) membrane winding with a new liner. As a first approach, the membrane material that is not qualified for further use, it undergoes a new dissolving process. Although it requires some re-work, the MEAs tested with the redissolved PBI batches showed as good results as compared to the pristine PBI

Tests were done with MEAs with defects (drag patterns, cracks, bubbles) and compared to MEAs with no defects and MEAs with deliberately made pin holes in the membrane (needle punched through). From this study is concluded that the severity of the defects was low on a short time scale. From the process development perspective, work was still done to remove the different defects from the membrane.

The QC waste came primarily from bubbles and defects created when winding up the finished membrane. A lot of effort was used to determine the severity of these defects and also to avoid creating them. Mechanical challenges with winding up the membrane on the coating and boiling machines were also a source of defects.

In view of the above, is possible to conclude that the overall waste % was reduced from 37% in 2017 to 24 % in 2019. The membrane material that could not be used directly was redissolved and new membranes coated from “rework” batches. This gave equally good membranes and same MEA performance as compared to pristine membrane material. This way the actual waste % of PBI material is close to 0%. The cost of reusing

the membrane material is actually lower than reuse of the Pt from the catalyst as the reuse process is shorter and only involves in-house process steps.

In addition to defect removal the membrane thickness is very crucial for obtaining a more uniform fuel cell performance and therefore the QC requirements for the thickness of the membrane has been increased from 2017 - 2021. In 2017 the QC requirement was a membrane thickness between 38 and 50 μm , but in 2018 the requirement was increased, and the membrane thickness was only allowed to be between 38 and 45 micron (ideally between 38 and 42 micron). See Figure 8.

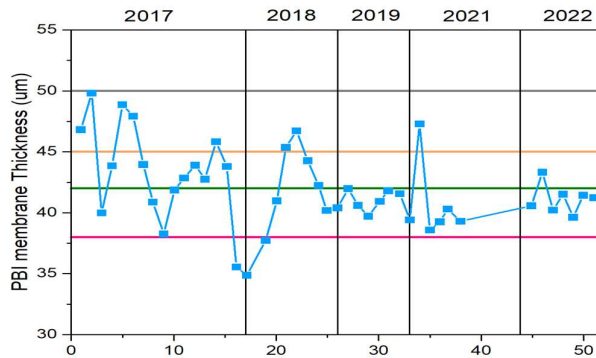


Figure 8. Membrane thickness of batches from 2017 to 2019. In 2019 all 8 batches were within the new QC limits. **Measured PBI thickness, lower limit 2017 -2021. Upper limit -2017. Upper limit 2018 -2019. Upper limit 2021**

The result of all the optimizations was a waste reduction of 50.6 % of the original waste in 2017. The process waste was reduced from 42.2 % to 28.1%, the geometrical waste was reduced from 15.1 % to 12.8 % and the QC waste was reduced from 42.7 % to 8.5 % (2019). Main focus in 2019 was the casting of membranes with a reproducible thickness (batch to batch) and on winding the PBI film with fewer imperfections such as bends or cracks. As seen in Figure 9 and similarly to the electrode upscaling, continuous effort is made to increase the PBI coating length while maintaining the standard variation below 2 %.

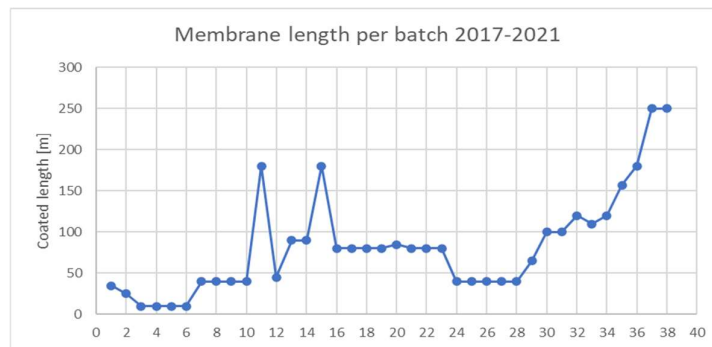


Figure 9. Overview of the achieved coating lengths over the period 2017 and Q3-2021

At the end of 2021, the process development started after the arrival of the new casting equipment at BWT facilities. The obtained membrane thickness using the established in-house manufacturing equipment is in the

range of 35 – 45 μm , with several batches in the range of 35 – 42 μm . This means that BWT has achieved low standard variation below 2% for 100 m coating runs



Conclusion: At present, the focus is to increase the coating length between 250 – 500 m with adequate uniformity below 2 % standard deviation. In this respect, the membrane waste is 100 % qualified for MEA production. However, and as a result of tighten quality control requirements, the PBI waste material has reached nearly 10 % (QC waste). This is attributed to dust embedded in the PBI coated materials during coating. BWT is working out on different approaches to address particle and dust entrainment issue.

Figure 10. image of the PBI coated material coated on PET substrate at BWT premises

MEA development

Pt load optimization below 1.4 mgPt/cm² on improved ink formulation.

The reduction of catalyst is a crucial task to reduce the cost associated to it. Optimization of the active sites (Pt wt%) concentration in the catalyst layer with respect to the amount of acid from the doped membrane can be attempted by partial substitution of the catalyst powder by carbon filler. The aim is to obtain same electrode thickness as the electrode E300 yet, with a decreased Pt Load.

The novel ink recipe with improved rheology properties was used for these test trials and the and the coating parameters were kept to the same values (flow rate, substrate speed) to obtain comparable electrodes. Good homogeneity and reproducibility were obtained during the fabrication of catalyst layers using the drum coater commonly used for small scale electrode coating. The scientific approach consisted in varying the catalyst loading in asymmetric systems (i.e., different loading in anode and cathode) as well as symmetric systems (i.e. same variation made at both anode and cathode in pairs).

All these investigations have resulted in different routes and methods enabling BWT to achieve the Cobra-Drive target of < 1.4mgPtCocm² total Pt load. As seen in Figure 11, the performance achieved in MEA-RD-21-171 is of 600mV at 0.4 A/cm². This means a 4 % voltage loss achieved with a significant reduction in the Pt loading of > 20%. (Figure 11)

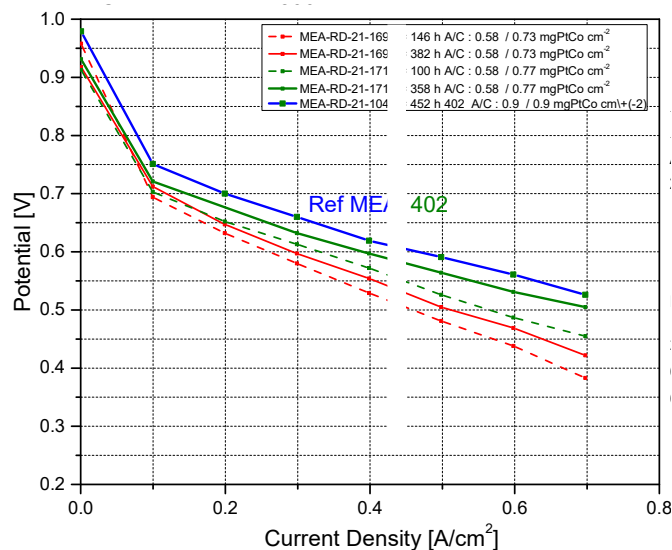


Figure 11. Polarization curves using varies combined anodes and cathodes with reduced Pt loading at $\approx 1.5\text{mgPtcm}^2$
 $\lambda_{\text{H}_2}/\lambda_{\text{Air}} = 1.3/2.5$, $T=160^\circ\text{C}$, Reformate fuel = 1.4% CO, 22.3 % CO₂, 69.3% H₂. Fixed water feed 6.1 $\mu\text{l}/\text{min}$

Conclusion: It has been proven that the catalyst loading can be substantially reduced > 20 % at an expense of 4 % voltage loss. The target of using less than 1.4 mgPt/cm² total has been achieved.

Single cell durability exceeding 10.000 h

Best performing MEA (402 type) was subjected to long term test at system operating conditions. figure 16, the degradation rate at 160 °C and constant load of 0.4 A/cm² was of 7.5µV/h over the first 9000 h. This is measured from Peak of Life (POL) value of 645 mV at approximately 300 h, and performance after 9000 h of 590 mV. After the 9000 h is possible to appreciate a step wise performance decreased due to a failure in air supply for 2 h, and therefore not related to the cell as such.

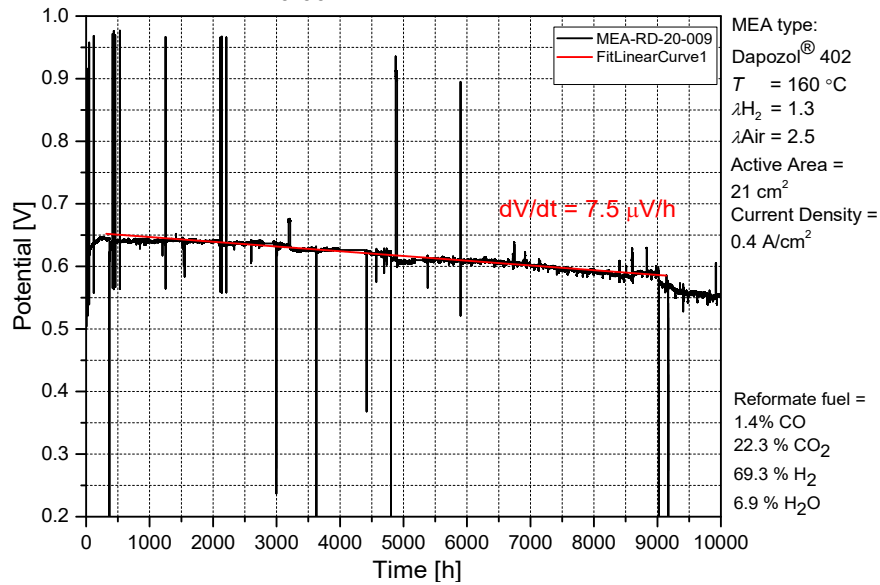


Figure 12. 10,000 hours durability test. Operating conditions: $\lambda_{H_2}/\lambda_{Air} = 1.3/2.5$, $T=160$ °C, active area = 21 cm², current density = 0.4 A/cm² Reformate fuel = 1.4% CO, 22.3 % CO₂, 69.3% H₂, 6.9% H₂O. Achieved project goal with 8.5 % voltage loss after 9000 h of operation.

Further validation of the in-house made 402 MEAs was made, exhibiting improved production robustness with an average voltage performance of 611 ±11 mV (See Figure 13)

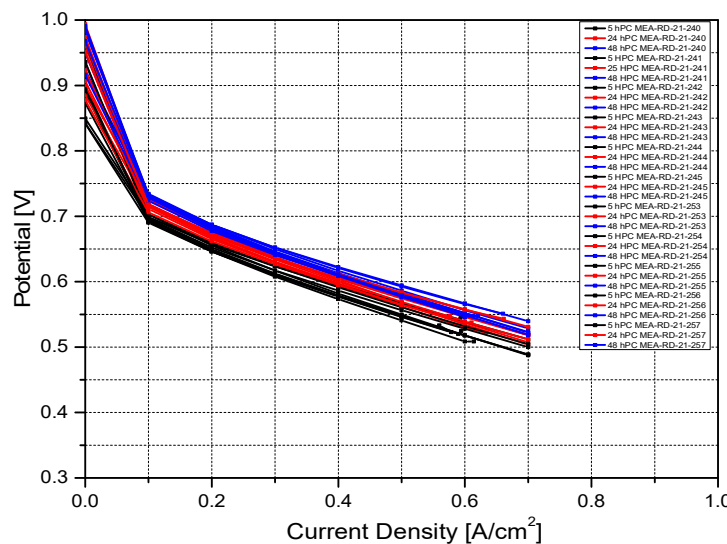


Figure 13. 402 Polarization curves recorded at 5-24-48 h, anode: Pt (LEC-15 – E), Cathode (LEC-17-E). $\lambda_{H_2}/\lambda_{Air} = 1.25/2.5$, $T=160$ °C, Reformate fuel = 1.4% CO, 22.3 % CO₂, 69.3% H₂, 6.9% H₂O. Fixed water feed 5.8 µl/min

Conclusion: the single cell 402 MEA type has exhibited durability of 10.000 h, at system operation conditions with a slight decrease of voltage loss of 8.5 % and thus achieving the project goal. Despite its relatively high loading, further optimization is currently being made to lower the total Pt loading based on 310 & 402 MEA product.

Results at stack level (G1018 402 MEAs)

After successful test on single cells (5x5 cm²) of the newly developed 402 MEAs, a step further has been done with the construction and building up of a large stack system consisting of 160 industrial cells with a total power output of 15 kW

The individual cell voltages are shown in Figure 14 and at a different current density. Remarkable results are obtained from mapping the performance of the individual MEAs (160) in the range between 0.1 – 0.6 A/cm². This is a major milestone achieved in the scope of the Cobra – drive project, with a successful demonstration of a 15 kW system where 100% are well-functioning MEAs. A number of full stacks are being built at the moment with the purpose of obtaining more statistics on stack measurements.

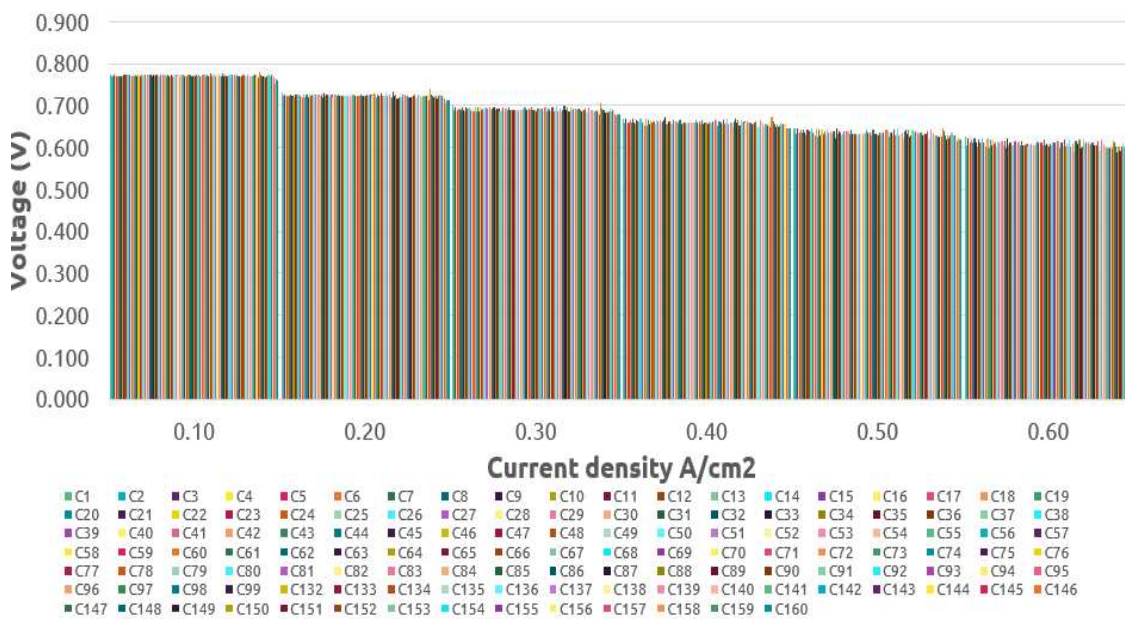


Figure 14. Voltage measurements obtained for 15 kW stack (160 cells).

Conclusion: The in-house coated material implemented in the 402 MEA type has resulted in the best performance ever measured at Blue World. One complete stack consisting of 160 cells showed 0% failure rate. Further work is being done to validate the MEA failure rate <0.1% in several stacks

Accelerated stress test to support MEA development.

Dilute effect and CO poisoning

The performance degradation of HT-PEMFCs was studied for the fuel impurities, at first the metal loading in the anode was reduced as already explored by the consortium. When operating with reformat fuel consisting of H₂, CO, CO₂, H₂O. The CO poisoning and dilution effect on HT-PEM fuel cells are studied in combination of varying Pt loaded anodes

Reference performance with pure hydrogen

Cell performance with pure H₂ as fuel is taken as a reference, which exhibits little changes in the fuel cell performance when platinum loading is reduced from 1.5 to 0.13 mgPt/cm², as shown in Figure 16. In the following study the CO content is varied 0.25 to 2.0%.

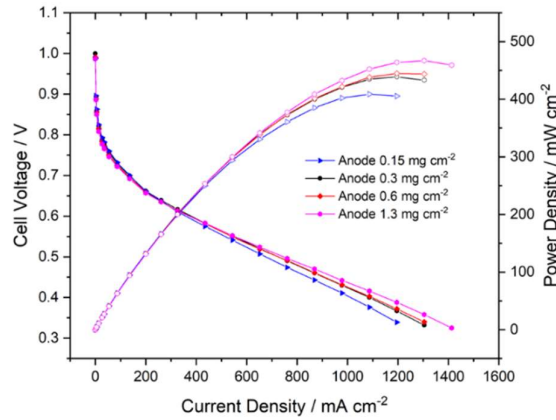


Figure 15. Influence of anode loading on cell performance. Cells are operated with pure H₂. Cathode loading= 1.3 mg cm⁻², T=160 °C, λ_{H₂} = 1.5, λ_{Air} = 2

3.1.1 CO poisoning at varied H₂ partial pressures and Pt loadings

The poisoning effect is studied when CO is added into pure H₂ (100%H₂) and 40%H₂-60%N₂ mixture fuels while the Pt loading of the anode is changed from 0.15 to 2.0 mgPt/cm². The results are shown in Figure 20. It is seen that, when operating on pure hydrogen, the poisoning effect of CO in the range of up to 2.0% is very limited at electrodes of high Pt loadings (e.g., 1.3 mgPt/cm²). This effect becomes severe when the Pt loading is decreased down to e.g., 0.3 mgPt/cm² and even more significant at the Pt loading as low as 0.13 mgPt/cm². Another finding is the CO poisoning is exaggerated when the hydrogen partial pressure is low, e.g., with 40% H₂ in N₂ as fuel. At low hydrogen partial pressures, the surface adsorption apparently favors for CO.

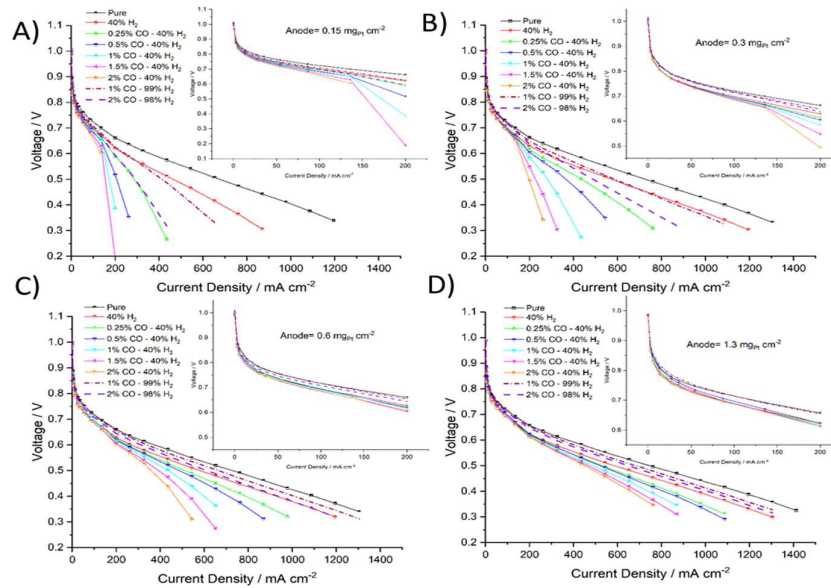


Figure 16. CO poisoning effects on polarization curves of fuel cells operating with 100% or 40% H₂. The anode Pt loading is changed from 0.15 (A), 0.3 (B), 0.6 (C) and 1.3 (D) mgPt cm⁻². Other test conditions are cathode loading = 1.3 mg cm⁻², T = 160 °C, λ_{H₂} = 1.5, λ_{Air} = 2

The two effects of the CO poisoning and H₂ dilution are summarized in figure 20 where the effects are represented by the cell voltage (V) at current density of 0.2 A/cm². In the figure the open bar is the reference performance for pure hydrogen, which has little changes with the Pt loading. The bars for 0%CO reflects the mere effect of H₂ dilution by 20-60% N₂. The dash-lined area on top of the bars indicates the CO poisoning, which is a function of the CO concentration, Pt loading and the H₂ partial pressure.

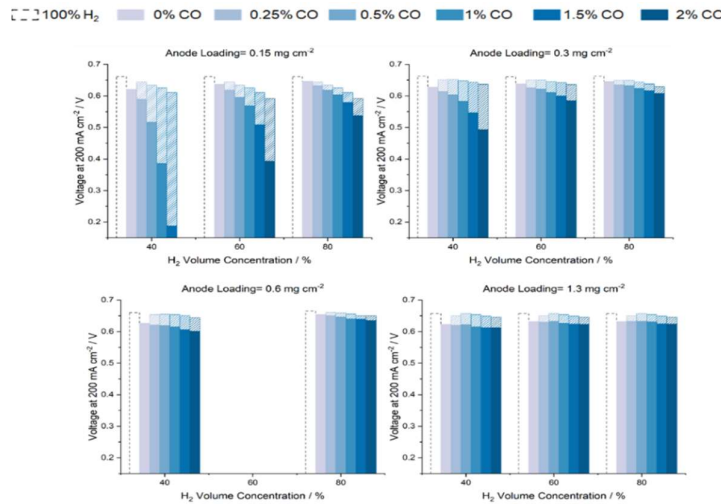


Figure 17. Impact of CO poisoning and H₂ dilution on the fuel cell performance at 200 mA cm⁻². Color filled columns depict CO poisoning and H₂ dilution. Summation of color filled and dashed columns depicts only CO poisoning. Cathode loading= 1.3 mgPt/cm², T=160 °C, λ_{H₂} = 1.5, λ_{Air} = 2

Conclusions: A number of literature studies have been published to explore the low to ultralow Pt loading electrodes, however, evaluated with pure hydrogen as fuel. This should be re-examined for the reformat fuel. The CO poisoning effect is more severe at low H₂ partial pressure, which is of practical importance when reformat fuel from a methanol reformer is used.

Acid redistribution

Phosphoric acid is the proton conducting electrolyte in HT-PEM. It is brought into the cell as the dopant of the membrane. It has been estimated that about 10% of the membrane doping acid is transferred into the catalyst layer during the cell assembling. This process is called the break-in or activation, which is a period of 200 to 1000 hours for the cell performance optimization. Attempt was made to investigate migration of the acid from membrane to other parts of the MEA. X-ray computed tomography (CT) was used to capture 3D images from a cross-section of an MEA (See Figure 19). It is found that the acid was possible to transfer from the membrane to the microporous as well as carbon fiber layers after assembling. This indicates that cracks and imperfections in the microporous layer may influences the acid loss in the fuel cell.

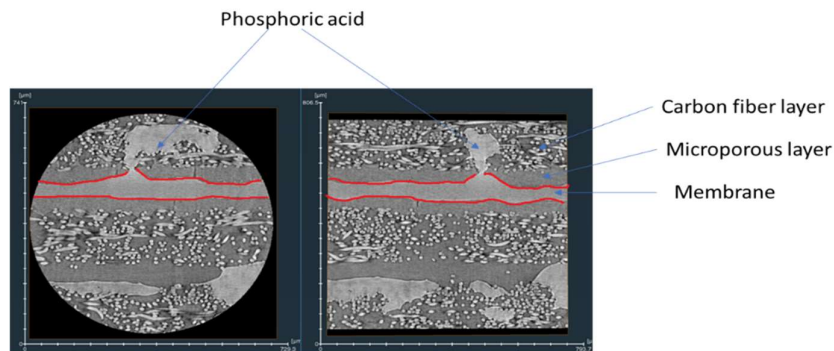


Figure 18. Impact of CO poisoning and H₂ dilution on the fuel cell performance at 200 mA cm⁻². Color filled columns depict CO poisoning and H₂ dilution. Summation of color filled and dashed columns depicts only CO poisoning. Cathode loading= 1.3 mgPt/cm², T=160 °C, λ_{H₂} = 1.5, λ_{Air} = 2

Acid condensation

Phosphoric acid has a very low vapor pressure at the fuel cell temperature. The vapor phase is nearly pure water with an acid content of the ppm level. The equilibrium water vapor pressure above phosphoric acid and acid doped PBI membranes is summarized in Figure 19. In other words, the acid condensation depends on the relative humidity of the atmosphere. For PA/PBI membranes at a typical acid doping level of 10, a minimum humidity of ca. 2% is needed prevent the phosphoric acid from condensation i.e., to maintain the acid concentration < 100% at 160°C (the red cycle point in the figure). Operating with dry hydrogen as fuel, this is fulfilled

at low stoichiometries of air, but the condensation may occur under idling or OCV. When operating with reformate fuel containing water, this may not be an issue. It is noted that the acid condensation may lead to significant performance temperature which is, however, recoverable after slow (hours to days) hydration of the cell.

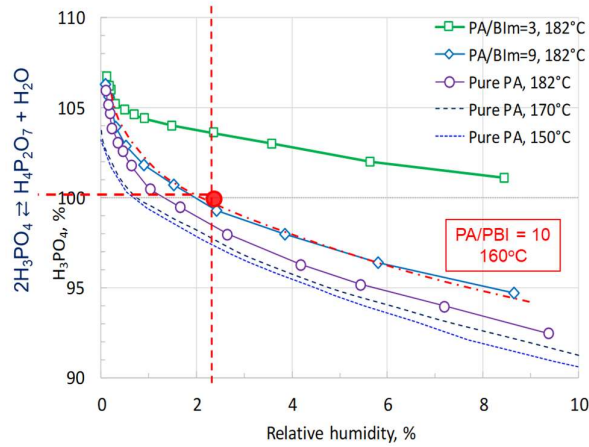


Figure 19. Isotherm hydration of phosphoric acid at varied temperatures and acid doped PBI

Acid losses via evaporation

The acid content in the vapor phase is found to be about < 1 ppm at 160°C and < 4 pm at 190°C, as shown in Figure 20. This may result in a significant acid loss for a lifetime of e.g., 40,000 hours when a huge amount of gases pass through the cell. A set of acid loss data for PBI cells as well as for PAFC is also shown in Figure 20, which closely follows the trend of the acid vapor pressure, indicating that the acid evaporation is a main acid loss mechanism. This is also the most critical issue of the long-term durability of PBI cells. As read from the figure, the acid loss rate is about 1 μg m⁻²s⁻¹ at typical fuel cell temperatures around 160°C. For BWT MEAS, the total acid inventory is about 20 mg H₃PO₄/cm². It is estimated that about 50% of the total acid might be carried away by the gas flow after 25,000 hours of operation, a critical issue identified.

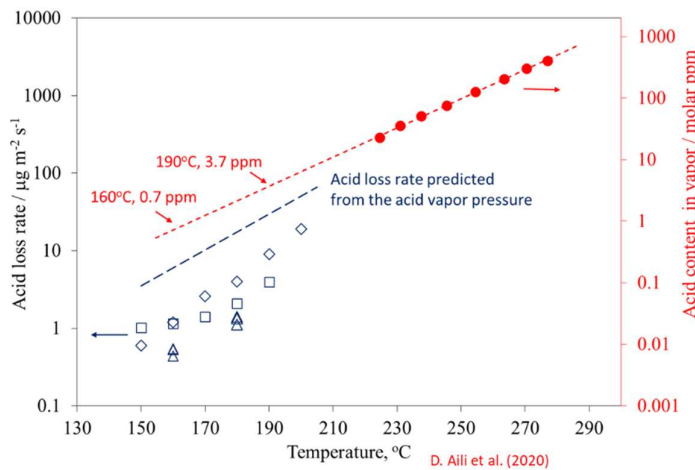


Figure 20. Prediction of the acid content in the vapor phase to the fuel cell operating temperature range and the measured acid loss rate at varied temperatures.

Conclusions: Acid undergoes a redistribution from the membrane to catalyst layers, as well as microporous and carbon fiber layers during the assembling. The acid condensation might be an issue under some circumstances. The acid loss via evaporation is a well-recognized mechanism of the fuel cell degradation.

Accelerated stress test - impact of operating conditions

Outline of degradation mechanisms

The identified degradation mechanisms include the acid loss via evaporation, catalyst particle growth and hence the reduced surface area and activity, polymer oxidation and thus membrane thinning as well as other component degradation such as gas diffusion layers and their hydrophobicity, bipolar plates, seals etc. Efforts are made to map of the impact of operating conditions e.g., temperature, current density, gas stoichiometry on the fuel cell durability, as reported in the following.

Stressors of temperature, current density and gas stoichiometry

During the AST, the temperature, current density and gas stoichiometry are used as the stressor. A typical set of I-V curves is shown in Figure 21.A for a steady state test duration of nearly 5000 hours test. The operating conditions are temperature of 160 °C, current density of 600 mA/cm² and low hydrogen stoichiometries of 2.0/1.6. From linear regression analysis, the ohmic resistance is obtained for each polarization curve. This is summarized in Figure 22, B together with measurements at 160°C but high gas stoichiometries (6.0/6.0) as well as at 160°C and medium gas stoichiometries (3.0/4.0).

The current density of 600 mA/cm² is already a stressor for the fuel cell durability, as well recognized in literature. It is obviously seen that the temperature is a much stronger stressor which changes the acid vapor pressure, platinum solubility, carbon corrosion, in addition to thermal and hydro stress at the MEA interfaces. At the same time the gas stoichiometries play also a critical role in deterioration of the fuel cell performance.

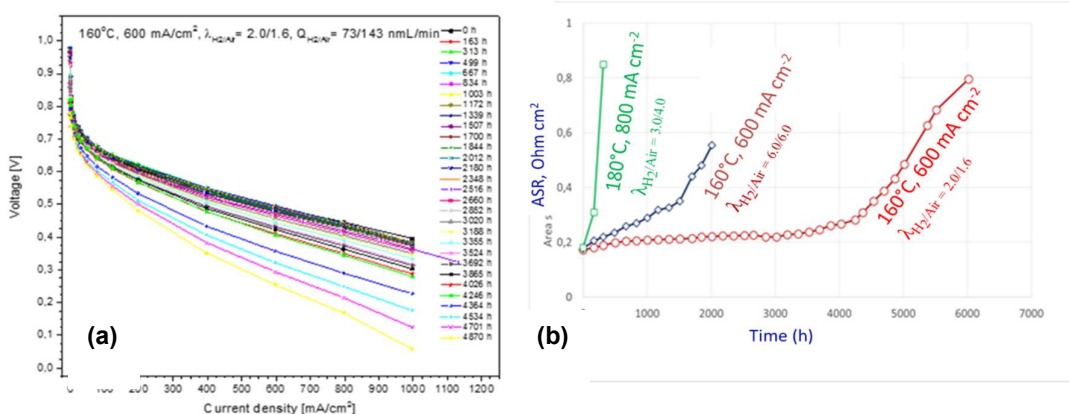


Figure 21. AST results at 160 and 180°C with varied air and hydrogen stoichiometries. A) polarization curves obtained within 4870 hours of operation at temperature of 160°C, current density of 600 mA/cm² and λ_{H₂/Air} = 2.0/1.6. B) Fuel cell ohmic resistance change in the lifetime test at 160 and 180°C, 600 mA cm⁻², and varied λ_{H₂/Air} stoichiometries from low (2.0/1.6) to medium (3.0/4.0) to high (6.0/6.0).

Catalyst degradation under potential cycling

Bu focusing on catalyst degradation the accelerated stress test is performed by square wave potential cycling between 0.6 and 1.0 V with a potential hold time of 8 seconds. During the cycling the anode is supplied with hydrogen while the cathode is supplied with nitrogen in either dry or humidified forms. I-V curves were recorded as a function of the cycling number of up to 30,000 cycles. It is found that the humidification strongly influences the potential cycling as an AST stressor for evaluation of platinum catalyst durability. No water is formed during the AST and the phosphoric acid condenses, which prevents the Pt dissolution and reprecipitation and hence the particle growth (Figure 22, b&d) in comparison with pristine catalysts (Figure 22, a). When the purging gas is humidified, platinum particles undergo an oxidation and dissolution during the high potential (1.0 V) period and reprecipitate during the low potential (0.6 V) period, which results in significant particle growth on the cathode side (Figure 22, c&e). This is the major mechanism of the electrode degradation when a fuel cell operates with start/stop or loading cycling modes.

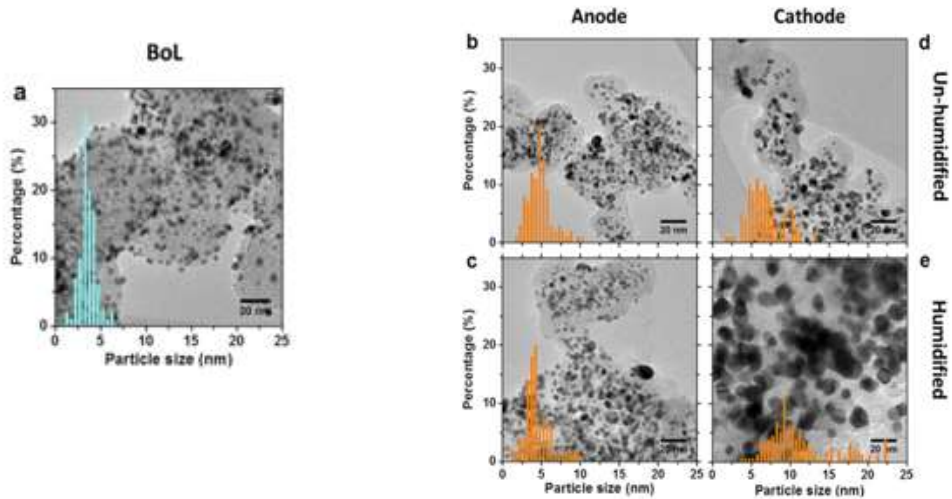


Figure 22. TEM images of Pt/C catalyst a) pristine catalysts; b) & c) anode after 30,000 cycles with unhumidified or humidified nitrogen. d) & e): cathode after 30,000 cycles with unhumidified or humidified nitrogen

Conclusions: major degradation mechanisms of PBI cell performance include the acid loss, catalyst particle growth and polymer oxidation. Of the AST stressors investigated, temperature is the most influential while current density and gas stoichiometry are also significant. Potential cycling is an affective AST tool for catalyst degradation study, in which the acid condensation or gas humidification should be carefully considered.

Addressing MEA cost target of 21 Euro

The execution of the Cobra – Drive project had resulted in great advancements in regard upscaling and manufacturing PBI membrane and electrodes. which has resulted in commercial 402 MEA pre-series. BWT is ramping up for mass-manufacturing in Aalborg with an annual production capacity target of 500MW/yr. The main drivers for MEA cost reduction are **a) Use of industrial production processes roll-to toll (R2R).** Successful installation and operation of the coating lines allows for the manufacturing of membrane and electrode materials thus entering into pre-commercial MEA **402 b) Reduction of critical raw materials (CRM).** This has been achieved and demonstrated within the scope of the Cobra-drive project showing MEAs below 1.4 mgPt/cm².

Figure 23 shows the MEA cost distribution based on its individual components: a) catalyst, b) membrane, d) gas diffusion layer and c) other supplies. The distribution of the cost based on the individual materials are presented for a demand scenario of 250,000 and 600,000 MEAs for 2023 and 2025. As observed, the Pt/catalyst cost represents a significant large share compared to the rest of materials included in the MEA. Looking at this figure, it seems obvious that the reduction of the metal content in the MEA is an important to address cost target. This assumption is valid if the MEA power output is not compromised because of such a reduction.

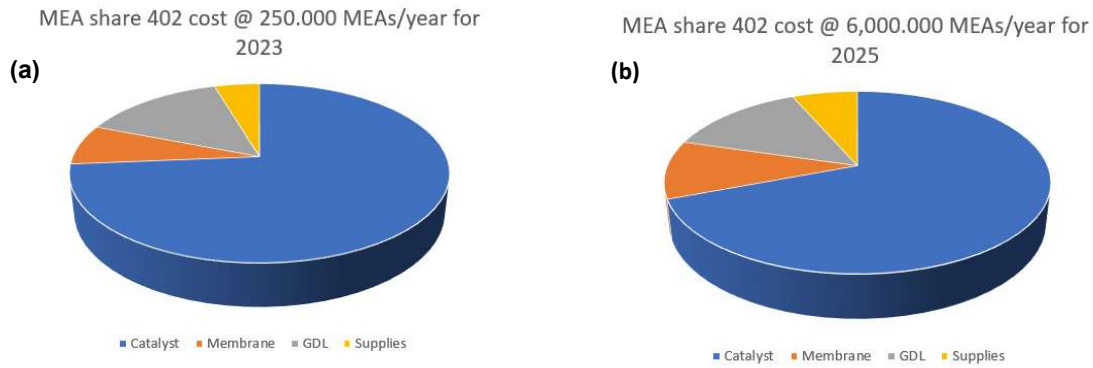


Figure 23. Pie chart showing the material price distribution at MEA level a) price cost distribution in 2023 and b) forecast in 2025 based on MEA demand

Lifting- up MEA power output. The investigation of different operation strategies has enabled greater performance for the 402 MEA type (i.e., increased pressure and/or temperature operation). A higher power output per MEA results in a shorter stack which results in fewer MEAs for the same power output. This strategy yields to a further reduction in the cost per produced kilowatt in the FC stack. As seen in Figure 24, the use of the enhanced operation (i.e., higher operational temperature or use of increased gas pressure) allows for a reduction of the power cost (Euro/kW) by nearly 46 % compared to nominal conditions which has been tested in the range of 1.4 – 1.6 mgPt/cm² total Pt load. The new operational strategies are being currently validated in lab 5x5 cm² MEAs.

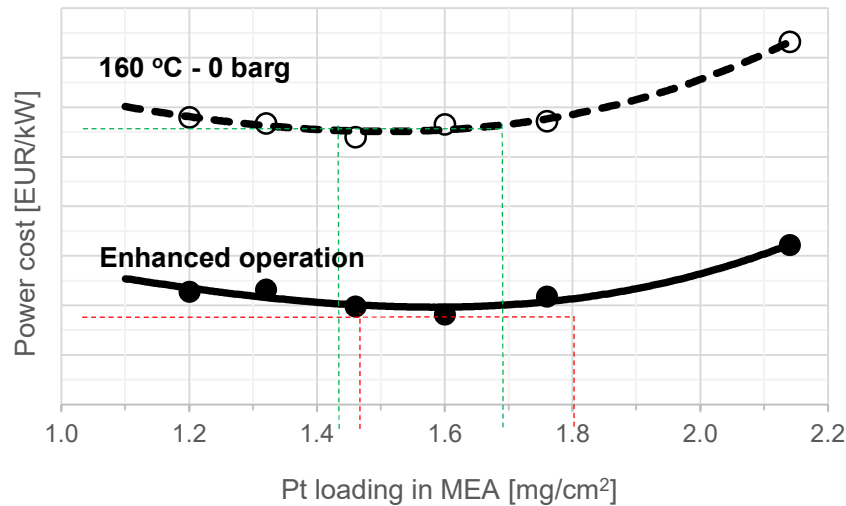


Figure 24. Power cost as function of the total Pt loading in MEA: (dotted line) nominal operation conditions, (solid line) at tested conditions in 5x5cm² lab size MEAs.

Conclusion: The combination of increased production volumes, reduction of the overall Pt load to a suitable range, and increased power output has resulted in a favorable economic scenario ² driving the MEA cost below 21 Euros even at production volumes of 100.000 MEAs/year.

In addition to the above-mentioned drives for MEA price reduction, BWT is testing cheaper and recycled catalyst material for MEA test & qualification. This is addressed as part of the product development activities in the aim to push further down the MEA cost.

² According to internal calculations and based on the estimated material prices at a different MEA demand scenarios

Table 3. Production volumes based on MEA demand for 2022 – 2023 – 2025 and estimation of the MEA cost based on nominal operating conditions and * enhanced operation mode.

Year	MEAs	Eur/kW (nominal operation)	Eur/KW *	Eur/MEA *
2022	100000	669.6	361.6	20.09
2023	250000	533	287.8	15.99
2025	600000	436.6	235.8	13.10

*Pressurization and increased temperature conditions. Total Pt load of 1.4 -1.6 mg cm⁻² (402 MEA)

Work package 3: Stack & Flow Plate Materials Development.

Utilizing the good properties of high temperature polymer electrolyte membrane fuel cells require special high-performance materials that are able to cope with the challenging operating conditions that exist within the HTPEM fuel cell stack. The bipolar plates need the following functionalities:

- Impermeability to gasses, including hydrogen.
- Good electric conductivity
- Resistance to uptake of liquids
- Chemical stability towards highly concentrated phosphoric acid
- Robust mechanical and thermal properties

This WP has included an exploration of new materials for processing bipolar plates, seeking to replace the BPPs currently used in the fuel cell stacks used in Advent's products.

This study ascertained that even though the plate performance parameters were ok for fuel cell operation, they did not provide good durability due to the removal of acid from the fuel cell membranes. Because the phosphoric acid present in the used polybenzimidazole membranes account for the majority of the proton conduction in the membrane, it is critical to keep this at a minimal loss, which was not the case with the phenolic resin plates. In large scale optimized fuel cell mass manufacturing, the use of metallic bipolar plates is usually a desired production process to exploit. With such techniques, cheap metallic foils can be used, which significantly can lower costs, weight and in turn yield superior power densities. Commercially advanced low temperature PEM fuel cell production has shown good performance using such techniques. But when considering the high temperatures and high phosphoric acid content of HTPEM fuel cells, such as Advent's; challenges with corrosion are extreme. It is not possible to use standard metals and stainless steels, a coating is needed that can handle to rough environment without compromising the surfaces of the BPP.

A significant understanding the raw materials and the processing used to make bipolar plates for high temperature PEM fuel cell stacks was achieved during the project. Important knowledge was obtained in examining CFD simulation as decision tool for further development of new bipolar plates for high temperature PEM fuel cell stacks.

This WP focused on construction a stack using Dapozol MEAs in the 165 cm² design matching the stack in the SereneU unit. Even though the BWT MEA and the standard production MEAs of Advent are both high temperature PEM fuel cells, several differences exist between the technologies both on membrane and electrode level. This needed special attention on stack level, in order to be able to assemble a functional stack of sufficient quality to be able to operate in a 5kW fuel cell unit. Different modifications were made to the 120 cell stack and flow plates, in order to enable the integration of the BWT MEAs.

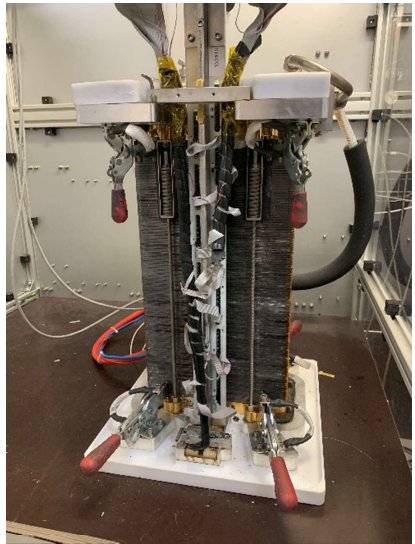


Figure 25: 120 cell stack undergoing testing after assembly in production test setup.

In Figure 25 **Error! Reference source not found.**, the assembled fuel cell stack can be seen, mounted in a production stack tester for performance evaluation and acknowledgement of problematic cells of assembly defects. Every single cell voltage is monitored during the course of fuel cell activation and submission to various test protocols, clearing the stack for operation in a SereneU unit.

Advent ordered 130 MEAs from BWT for integration in a demonstration stack. MEAs can be seen in figure 1. Some of the MEAs in the received batch showed some problematic performance in the factory acceptance test. These problems were sorted out and repairs introduced to mitigate the problems. The resulting stack was of an acceptable quality to move into further testing in a SereneU prototype unit.



Figure 26: HTPEM MEAs in the 165cm² format used in SereneU systems assembled in Aalborg

Work package 4: RMFC Core Optimization

Advent's fuel cell unit operates with a methanol/fuel mixture, but conversion to a hydrogen rich gas is needed for the high temperature PEM fuel cells to produce electricity efficiently. The conversion of fuel is carried out through a steam reformer, converting the methanol and water into a resulting gas consisting of hydrogen, CO₂, CO, water and small amounts of unconverted methanol. The quality of the resulting gas is an important factor that contributes to the lifetime of the fuel cell stack.

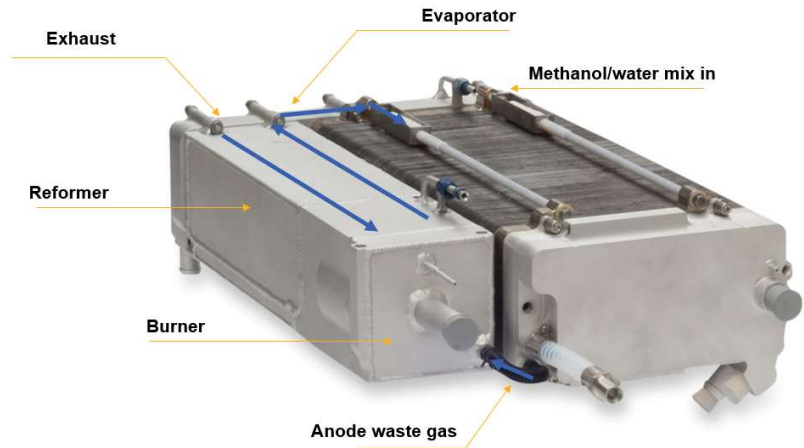


Figure 27: Advent's H3-5000 reformer

When increasing the flow rate of methanol from 4.5 L/h to 6.75 L/h (with S/C = 1.3), the temperatures in both tube and shell sides are decreased because more energy is consumed in the catalyst bed. The hydrogen concentration in the reformat gas is slightly reduced.

According to modelling data, the start-up process can be further studied and optimized going forward, to minimize the start-up time, minimizing the CO concentration in the reformat gas, and realize high efficiency and stable operation of the reformer.

In order to achieve the durability targets of light commercial vehicles, the reformer of the H3-5000 needed to be redesigned and optimized. The optimization target was to decrease the amount of unconverted methanol being output by the reformer over the lifetime of the reformer system. In turn this would improve the quality of the gas going into the fuel cell stack, increasing the general lifetime of the fuel cell system in its entirety. Figure 28 shows the results of the different reformer redesigns on the reactor methanol slip as a function of operating hours. The development activity and different generations of reactor developed lead to a superior design, eventually performing well above the original design targets.

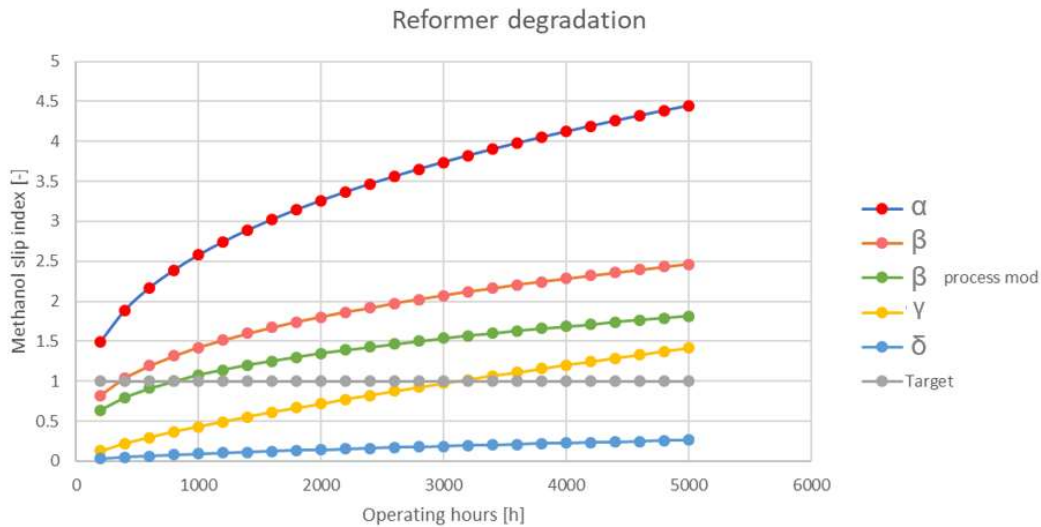


Figure 28: Graph of the methanol slip index of the reformer, showing experimental results of different reactor designs.

Work package 5: System Optimization.

Several activities were undertaken to improve module lifetime and quality, also on system level, an example of this is the engineering efforts undertaken to improve parts of the cooling system for achieving better dynamic performance of the fuel cell stack cooling system.

Examples of SereneU fuel cell system optimizations include:

- Trials of improved cooling system piping, significantly improving manufacturing ease
- Redesigned fuel injection system, improving durability and performance at low flow
- Optimization of total system flow control and hydrogen anode gas
- Trials of coolant system flow control using faster acting valves

In total these different, and more system improvements have been validated for several thousands of hours in-situ in running modules, 24 hours per day, all days of the year.

Work package 6: System Reliability.

For the reliability of a hybrid high temperature PEM fuel cell-battery system, understanding the degradation mechanisms of all components is the first step. In this project the focus is on improving the reliability of the reformed methanol fuel cell system, which is a tightly integrated system made up of a methanol-steam reformer (MSR) and a high temperature PEM fuel cell (HT-PEMFC). Therefore, to investigate the reliability of such a system the main components of the system, namely the fuel cell stack and the methanol-steam reformer were modeled and characterized separately.

Fuel cell reliability

To assess the reliability of current High temperature PEMFC technology, a literature survey on the HT-PEMFC degradation mechanisms was done and a lifetime prognosis model that can help predict degradation patterns was prepared based on literature data. The model focuses on the activation and ohmic losses, and investigates the evolution of these losses in time, depending on the different factors that affect them. The activation losses were defined as a function of changes in time of the mass of the active catalyst area to account for catalyst loss as well as changes in the average diameter of Pt particles to account for particle agglomeration. The simulations revealed that electrochemical active surface area (ECSA) loss is a major contributor to the total voltage loss, while the loss of conductivity increased significantly on a percentage basis over time, but still has a fairly low impact on the overall total voltage degradation. The ohmic losses were defined as a function of changes of acid doping level in time. It was found that the evaporation of phosphoric acid causes the ohmic overpotential to increase, especially at temperatures above 180°C. Therefore, higher temperatures can lead to shorter lifetimes but increase the mean output power over the lifetime of the fuel cell owing to higher performances at higher temperatures. Lifetime prognosis was also done at different operating temperatures. It was shown that while the fuel cell performance increases linearly with increasing temperature at the beginning of life, the voltage decay rate increases exponentially with increasing temperature. Based on analysis on voltage decay rate and lifetime prognosis, the operating temperature range between 160°C and 170°C can be said optimal, as there is a significant increase in performance compared to lower operating temperatures without too much penalty in terms of lifetime. The time-dependent cell performance was modeled as follows:

$$E_{cell} = E - \eta_{act}(t) - \eta_{ohm}(t) = E - A \ln\left(\frac{i}{i_0 a(t)}\right) - \frac{\delta m}{\sigma_m(t)} i \quad (1)$$

$$a(t) = \frac{m_{active}(t)}{A_{geo}} \frac{3}{\rho_{Pt} \frac{d(t)}{2}} \quad (2)$$

where A is the Tafel slope and a , δm , σ_m , m_{active} , A_{geo} , ρ_{Pt} and d are the degradation factor, membrane thickness [cm], membrane conductivity [S/cm], active mass of Pt [g], geometric area [cm²], density of Pt particle [g/cm³], and the average diameter of Pt particle cm, respectively. There overall model schematic is shown in Figure 29.

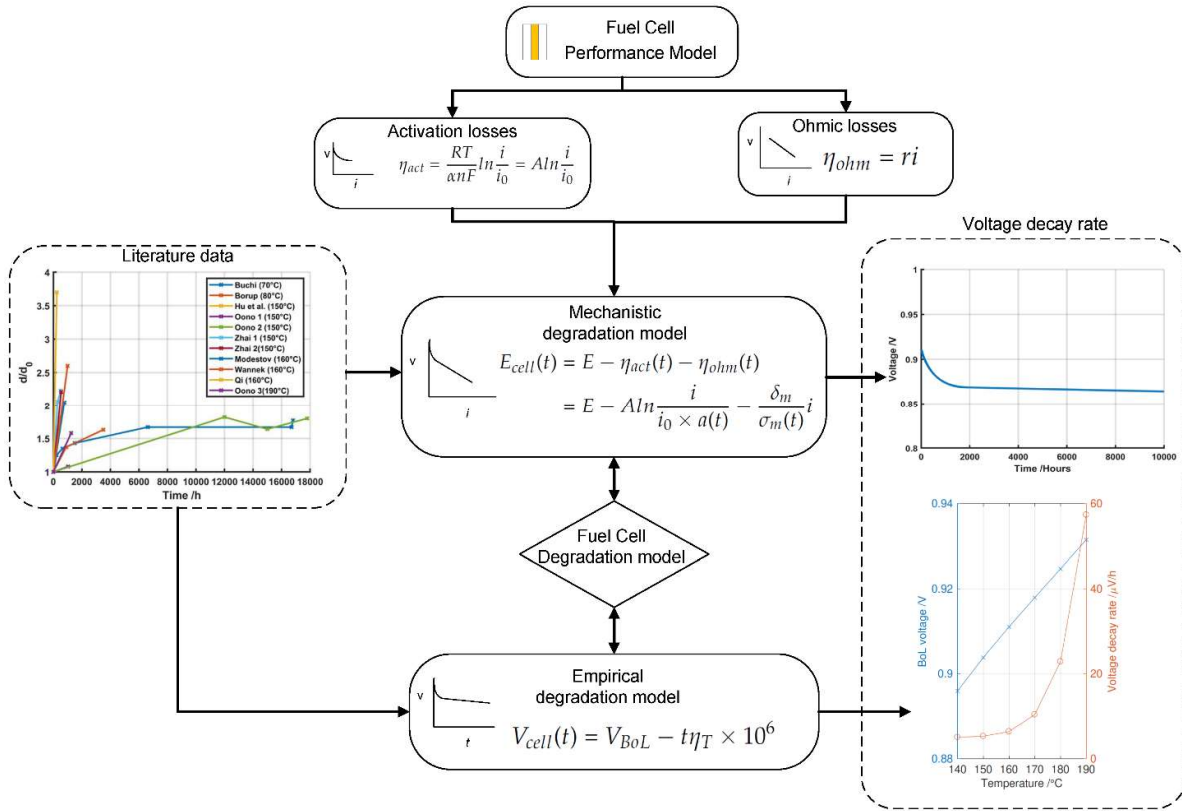


Figure 29: Schematic of the degradation model.

The degradation model is based on a literature survey given in table 1.

Table 1. Literature survey of HT-PEMFC degradation data. std is recommended standard operating conditions (160°C, 0.2 A/cm², 1 atm, λ_{anode}/λ_{cathode} = 1.2/2), ss is steady state operation, t is time (durability test), T is temperature, cyc is cycling operation and reformatate refers to the hydrogen-rich gas produced during methanol steam reforming process.

Table 4: Literature survey of HT-PEMFC degradation data.

Reference	Investigated Parameter	Voltage Decay Rate [$\mu\text{V}/\text{h}$]	T [$^{\circ}\text{C}$]	i [A/cm^2]	$\lambda_{anode}/\lambda_{cathode}$	Cycling/ Steady State	Fuel [h] or [number of cycles]	Duration	MEA
BASF [25]	t	6	std	std	std	ss	H ₂		
	cycle	47	std	std	n/a	2 h on/ 2 h off	H ₂	200 cyc	P1000
	cycle	35	std	std	n/a	2 h on/ 2 h off	H ₂	200 cyc	P1100W
Galbiati et al. [26]	t	8.6	std	std	std	ss	H ₂	950 h	P2100
	T	19	180	std	std	ss	H ₂	400 h	P2100
	i	4.5	std	0.4	std	ss	H ₂	800 h	P2100
	λ_{air}	8.5	std	std	1.2/4	ss	H ₂	800 h	P2100
Hu et al. [5]	t	150	150	0.64	n/a	ss	H ₂	500 h	own
Simon Araya et al. [27]	t	5	std	0.22	1.2/4	ss	H ₂	123 h	Celtec-P
	fuel impurities	900	std	0.22	1.2/4	ss	5% CH ₃ OH/ H ₂ O	400 h	Celtec-P
	fuel impurities	3400	std	0.22	1.2/4	ss	8% CH ₃ OH/ H ₂ O	200h	Celtec-P
Modestov et al. [28]	t	25	std	std	1.3/1.8	ss	H ₂	780 h	own
Moçotéguy et al. [22]	t	41	std	0.4	1.4/2	ss	reformate	1105 h	P1000
Moçotéguy et al. [23]	t	35	std	std	std	ss	reformate	total: ~650 h	P1000
	cycling	139/117	std	0.2/ 0.4	std	6 h 0.2/ 6 h 0.4	reformate		P1000
	cycling	54/ 26	std	0.2/ 0.4	std	12 h 0.2/ 12 h 0.4	reformate		P1000
	cycling	67	std	std	std	12 h on/ 12 h off	reformate		P1000
Oono et al. [29]	T	3.6	150	std	3.7/3.7	ss	H ₂	>16000 h	own
	T	13	170	std	3.7/3.7	ss	H ₂	6400 h	own
	T	59	190	std	3.7/3.7	ss	H ₂	1220 h	own
Oono et al. [17], Oono et al. [19]	t	3 (<14000 h); 9 (>14000 h)	150	std	3.7/3.7	ss	H ₂	17860 h	FuMA-Tech
Schmidt and Baumeister [30]	t	20	180	std	std	ss	H ₂ + H ₂ O	~200 h	P1000
	fuel impurities	20	180	std	std	ss	reformate	200 h	P1000
	fuel impurities	20	180	std	std	ss	reformate + Sulfur	3200 h	P1000
Schmidt and Baumeister [8]	t	5	std	std	std	ss	H ₂	6,000 h	P1000
	cycle	11	std	std	std	12h on/ 12h off	H ₂	240 cyc	P1000
Kannan et al. [20]	t	13.25	140	0.25	1.25/2.5	ss	reformate	>1600 h	P1100W
	i/cycling	11	120-180	0.03	1.25/2.5	cyc	reformate	4160 h, 1562 cyc	P1100W
	i/cycling	26	120-180	0.25	1.25/2.5	cyc	reformate		P1100W
	i/cycling	133	120-180	OCV	1.25/2.5	cyc	reformate		P1100W
Wannek et al. [31]	t		std	std	2/2	ss	H ₂	1000 h	custom FuMA-Tech
Wannek et al. [32]	t	25	std	st	2/2	ss	H ₂	>1000 h	FuMA-Tech
	t	20	std	std	2/2	ss	H ₂	order of hundreds	FuMA-Tech
	i/cycling	180	std	std	2/2	load variation	H ₂		FuMA-Tech
	cycling	120	std	std	2/2	off 1/d	H ₂		FuMA-Tech

Activation losses

Particle agglomeration

Based on data from literature an empirical model was prepared for the evolution of Pt electrocatalyst particle diameter. This is the main factor that affects activation loss, and therefore, its effects and evolution in time is added to the activation loss in the fuel cell performance increase.

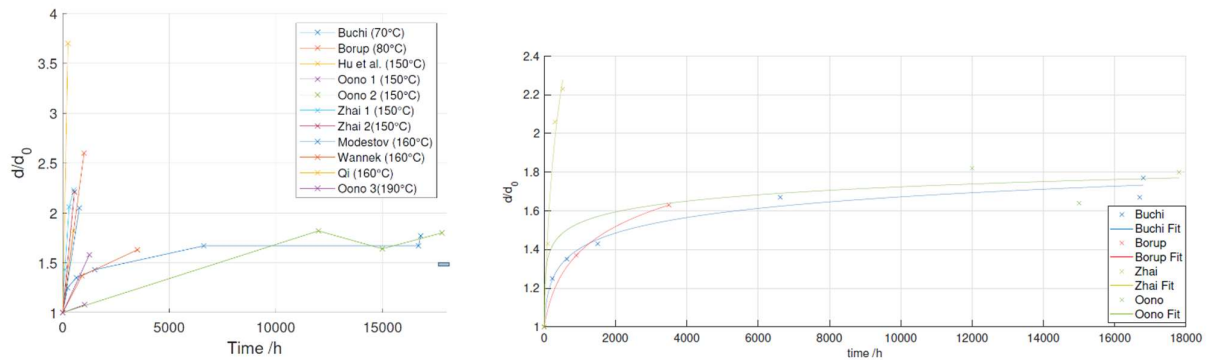


Figure 30: Evolution of Pt particle diameter in time. (a) Experimental data (b) Logarithmic fit of d/d_0 over time.

The evolution the of the Pt diameter is given as follows:

$$\frac{d}{d_0}(t) = a \ln(b(t + c)) \quad (3)$$

The dependence of Pt particle diameter on temperature is given by:

$$\frac{d}{d_0}(t) = aT + b \quad (4)$$

Based on the developed model the dependence of Pt diameter on time and temperature is shown in Figure 30b and Figure 31a.

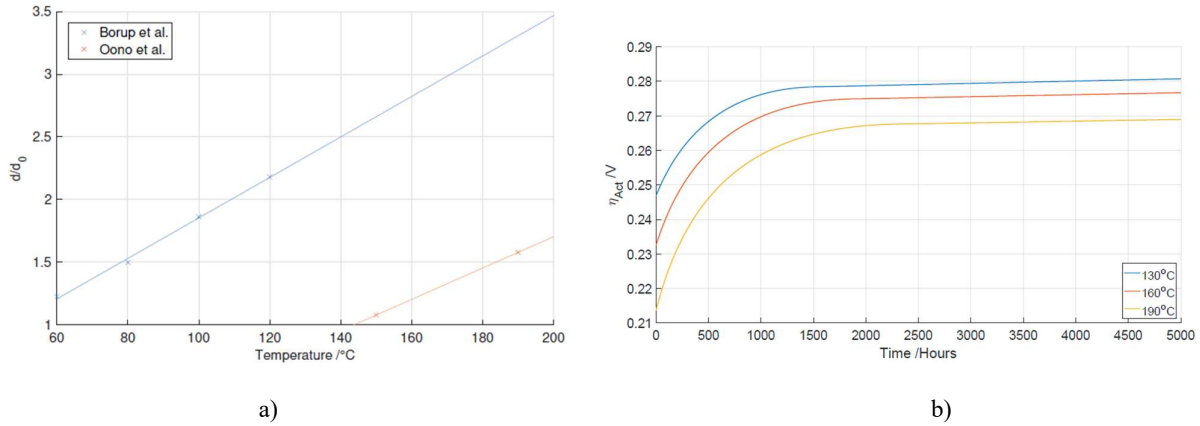


Figure 31: Evolution of d/d_0 and its dependence on temperature and its effects on activation loss. (a) Ratio d/d_0 as a function of temperature (b) (a) Temperature dependency of activation losses over time

Consequently, as a results of the evolution of the Pt electrocatalyst particle diameter the activation loss with time at different temperatures is shown in Figure 31b.

Ohmic losses

Acid loss

The ohmic losses of the fuel cell were assumed to heavily depend on the phosphoric acid loss from the fuel cell during its lifetime and modelled as such.

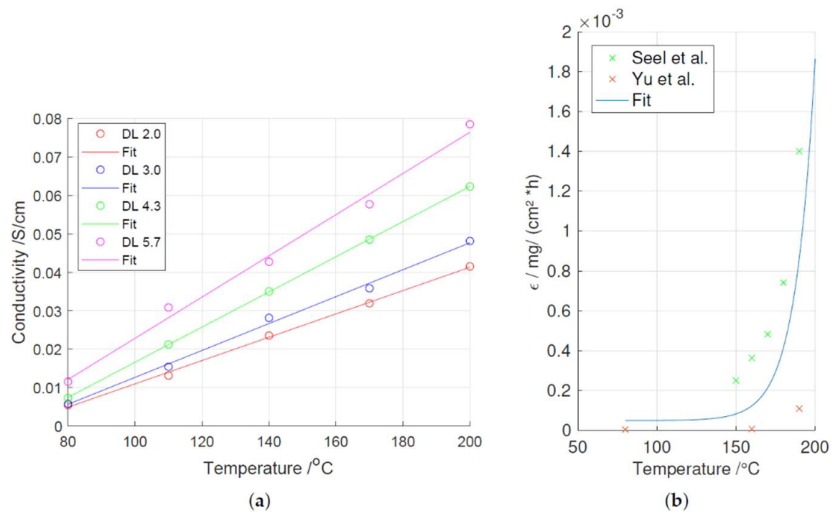


Figure 32: Temperature dependency of ohmic losses over time. (a) Conductivity of PBI - H₃PO₄ at different doping levels (DL) and temperature together with fits (b) Phosphoric acid evaporation rate as a function of temperature

Figure 32 shows the model fits with literature data of PBI conductivity and acid evaporation for different operating temperature. The overall time and temperature dependency of the ohmic losses can then be modelled based on the acid loss. Figure 33 shows these trends for different operating temperatures.

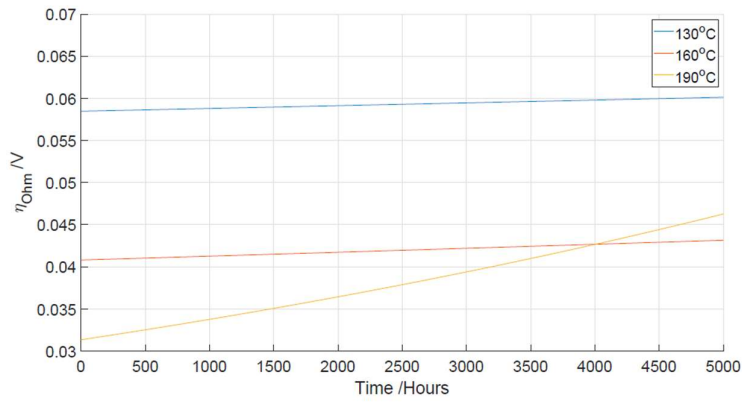


Figure 33: Ohmic overpotential over time as a function of temperature

Lifetime prognosis

Finally, adding both activation and ohmic losses to the performance model and overall degradation model of the fuel cell can be generated and used for lifetime prognosis. The cell voltage decay over time is shown in Figure 34.

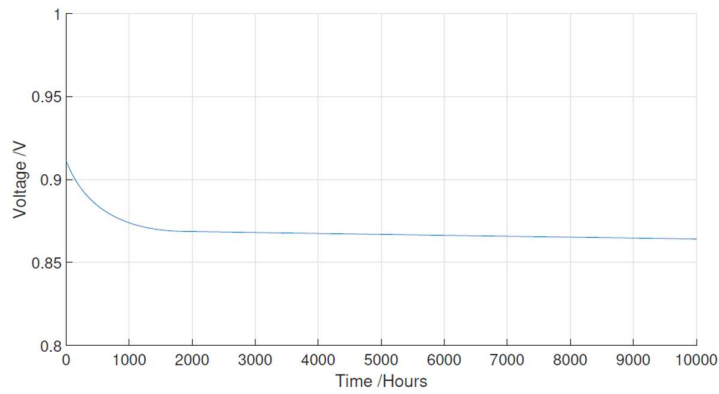


Figure 34: Cell voltage over time at 160°C.

By plotting the biggening of life (BOL) and degradation rate are plotted as a function of temperature, a lifetime prognosis can be done, and optimal operating temperature can be identified in terms of performance and durability.

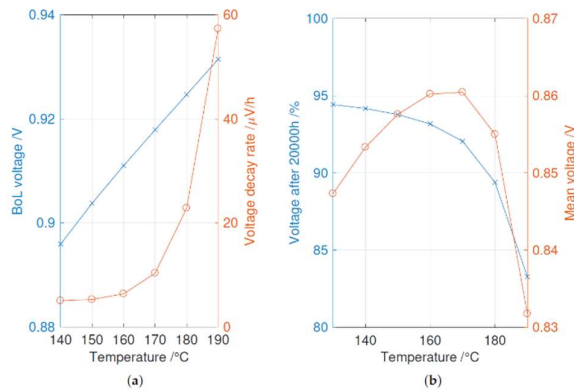


Figure 35: Voltage decay rates and lifetime prognosis. (a) BoL voltage and decay rates as a function of temperature (b) Cell voltage after 20000 h and mean operating voltage as a function of temperature.

As can be seen from Figure 35, the operating temperature range between 160°C and 170°C can be said optimal, as there is a significant increase in performance compared to lower operating temperatures without too much penalty in terms of lifetime like the higher operating temperatures (> 180°C).

Startup/shutdown and load cycling test protocol

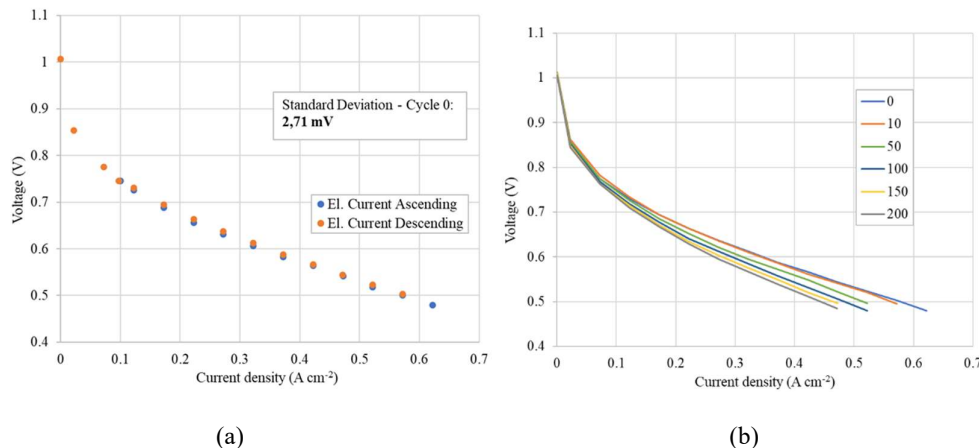
A start-up and shutdown procedure and load cycling were established to simulate real operating conditions in current commercial FC systems (e.g., without nitrogen purge). The upper current limit was generally set to "expected > 0.50 V" over the MEA while the polarization curve was measured. The change of current load was always done with a function of ramp (max. 1 A s⁻¹), while the mass flows are automatically adjusted according to the stoichiometry. This is especially the case when increasing the electrical current, where the flows are adjusted prior to changing the current to prevent reactant starvation in the FC. The test procedure and parameters are given in Table 5.

Table 5: start-up and shut down cycle by steps

Step	Time	Temperature °C	Flow anode dry Nlmin ⁻¹	Flow cathode Nlmin ⁻¹	Current density Acm ⁻²
1	Heating up	ramp to 120	0	0	0
2	Fuel flush for 5 sec	120	222	0	0
3	Heating to > 157 °C Gas flow settings	ramp to 160	λ 1.25	λ 2.5	0.1
4	OP Load time = 30 min	160	λ 1.25	λ 2.5	0.4
5	EIS measurement	160	λ 1.25	λ 2.5	0.4
6	Polarization curve	160	λ 1.25	λ 2.5	Ramp to max. El. Current*
7	Load time = 15 min (stabilization)	160	λ 1.25	λ 2.5	0.4
8	Cooling down	ramp to 120	λ 1.25	λ 2.5	0.1
9	Stop air flow, 10 sec [@]	120	0.078	0	0.05
10	Stop all flows, Consume H ₂ for 10 sec	120	0	0	0.01
11	Dwell	Ramp to < 50 °C (or RT)	0	0	If U > 0.5 V, set q to 0.01 Acm ⁻²

Figure 36a shows the standard deviation of the polarization curves measured according to the activation protocol and

Figure 36b polarization curves for different start-stop cycles. Even though, IV curves were recorded after every 10 start-stop cycles, only the polarization curves after 0, 10, 50, 100 and 200 start-stop cycles are plotted for clarity. It can be clearly seen that the voltage drops significantly due to the degradation caused by the start-stop operation of the cell. The EIS measurement and the voltage with increasing start-up/shutdown cycles are also shown in Figure 36c-d. The total degradation after all 200 completed start-stop cycles is -49 mV, while the average degradation rate per 1 cycle is approx. -0.25 mV.



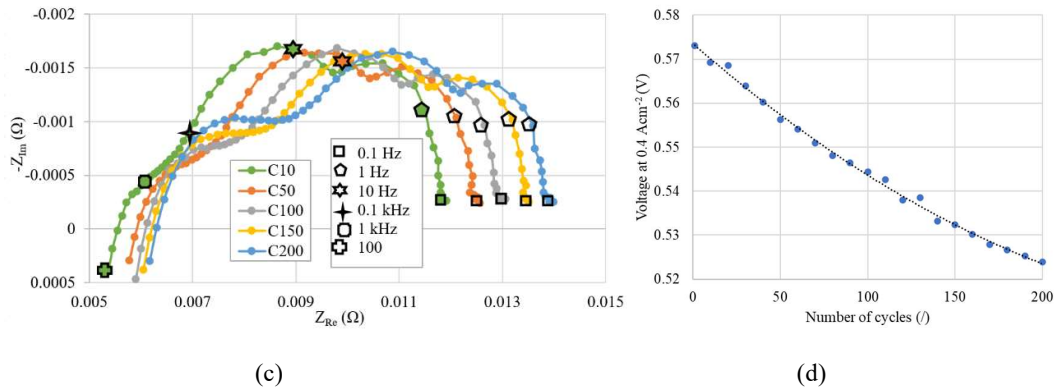


Figure 36: (a) Polarization curve taken after the activation protocol (before start-stop cycling) with calculated standard deviation. (b) Polarization curves after 0, 10, 50, 100, 150, 200 start-stop cycles. (c) EIS measurements under start-up/shutdown cycling. (d) cell voltage at different start-up/shutdown cycles.

Fuel cell stack level reliability

The reliability of a fuel cell system among other things depends on its robustness towards impurities that are inherently present in the output of the methanol-steam reforming process, which gives hydrogen-rich gas mixture known as reformat. Other than the desired hydrogen product, the reformat also contains impurities such as CO₂, trace of CO and unconverted methanol and water vapor.

In this project the effects of all the reformat constituents were tested on two types of fuel cell stacks delivered by Serenergy A/S. While in literature the effects of these contaminants are investigated mainly at single cell level and in dry conditions, for a proper transition of the technology to real life application, the tests in this project were done at stack level and in humidified conditions. This way, along with the impurities, the effects of water vapor, which is always present in the reformat mixture have also been characterized.

The two types of stacks used in the project differ in the type of phosphoric acid doping techniques used and in the gas diffusion layer (GDL) manufacturing process, two parameters that have implications both on durability and cost. The first stack was made up of post-doped PBI membrane with non-woven type of GDL in the membrane electrode assembly (MEA), while the second stack consisted of pre-doped membrane and a woven GDL. The two stacks used in the work consisted of 37 cells each with an active area of 165 cm². A schematic of the test setup and a photo of one of the stacks is shown in Figure 37.

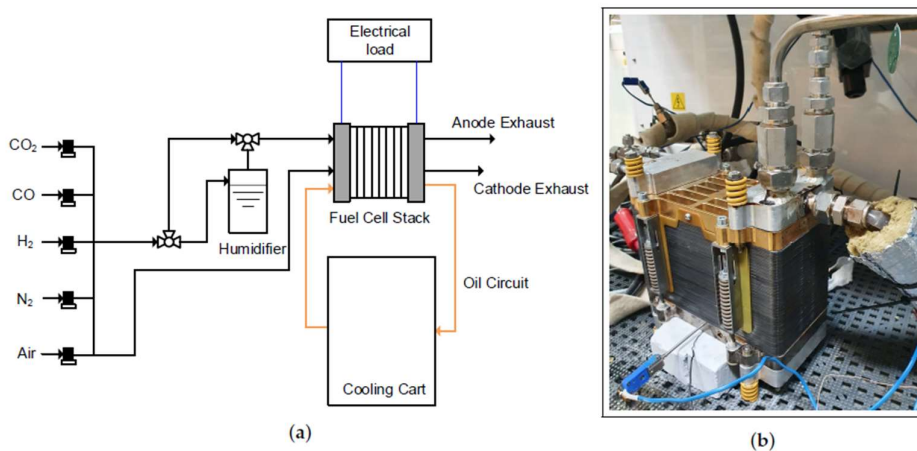


Figure 37: Test setup used for the experimental investigation of the two fuel cell stacks (a) A schematic of the test set up (b) One of the Advent fuel stacks used in the investigation.

The stacks were run according to the test procedure in Table 6: Test procedures and were exposed to the different operating conditions and gas compositions. Polarization curves and electrochemical impedance spectroscopy (EIS) were used to characterize the effects of the different operating conditions.

Table 6: Test procedures

Test Step	Anode Gas Composition	Duration
Break-in	100% H ₂	50 h
Nitrogen dilution	100% H ₂ , 31.7% N ₂	24 h
Dry reformate	68.3% H ₂ , 0.9% CO, 21.8% CO ₂ , 9% N ₂	24 h
Air-bleed	2% air, 98% H ₂	5 min
Wet reformate	68.3% H ₂ , 0.9% CO, 21.8% CO ₂ , 9% H ₂ O	24 h
Air-bleed	2% air, 98% H ₂	5 min
End of test recovery	100% H ₂	24 h

From the results shown in Figure 38a, it can be seen that the performance of the stack with post-doped membrane and non-woven GDL decrease with the introduction of the reformate impurities compared to initial pure and dry hydrogen test. The effects are similar whether the impurities are humidified or not, and the performance decay due to impurities is highest at the beginning of test for both dry and wet reformate operations. From the Nyquist plot representation of the impedance measurements, it can be seen that while the effects of the impurities stabilize after 24 hours of test for the dry reformate operation, however, despite a slight recovery in the beginning the degrading effects continue to exacerbate for the humidified operation, especially on the low frequency region. Pure and dry hydrogen operation at the end of test shows that the performance losses are recoverable to a high degree, which could lead to believe that pure hydrogen operation (or perhaps inert gas flushing) at certain intervals could be considered a recovery mode and could avoid severe irreversible degradation.

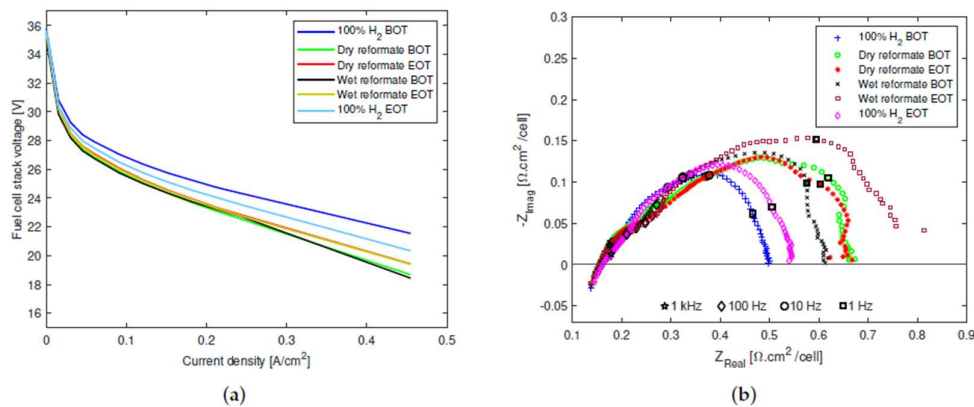


Figure 38: The effects of dry and wet reformate impurities on an HT-PEMFC stack with an MEA composed of a post-doped PBI membrane and non-woven GDL. (a) Polarization curves. (b) EIS spectra.

Similarly, the effects of the impurities are also clearly visible on the stack with MEAs made up of pre-doped membranes and woven GDLs, Figure 39. However, unlike for the post-doped MEAs humidification alleviated the effects of the impurities as can be seen from the slightly improved performance under wet reformate compared to dry reformate operation at higher current densities, shown in Figure 39a. It can also be seen in Figure 39b that the EIS spectra shrink in size in the low frequency region upon humidification, indicating that mass transport losses are reduced. Moreover, the dry and pure hydrogen operation at the end of tests results in an even higher performance recovery in this case compared to the stack with post-doped MEAs.

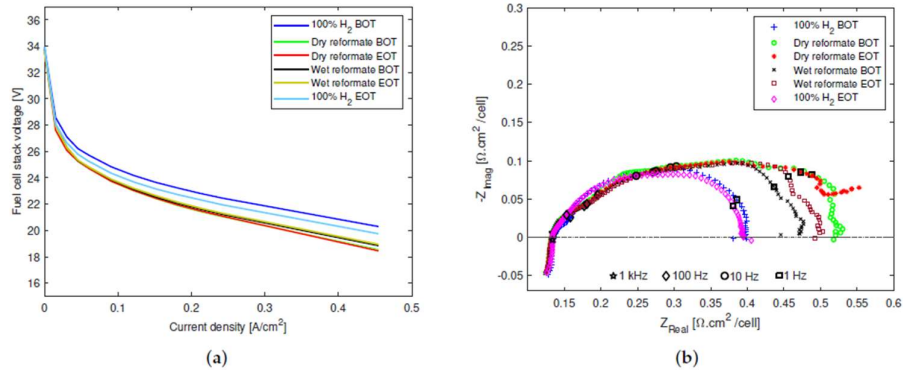


Figure 39: The effects of dry and wet reformate impurities on an HT-PEMFC stack with an MEA composed of a pre-doped PBI membrane and woven GDL. (a) Polarization curves. (b) EIS spectra.

Reformer reliability and optimal design

1D reformer model

In order to enhance the performance and robustness of the methanol steam reformer, it is important to understand the underlying kinetic behavior of the reforming process. Therefore, modeling and experimental work was done on a multi-tubular packed-bed reformer with estimation of effectiveness factors for methanol steam reforming over Cu/ZnO/Al₂O₃ catalyst.

Steady-state models has been developed to describe the kinetic behavior of a commercial Cu/ZnO/Al₂O₃ catalyst BASF BK10, taking into account the kinetic reactions and effectiveness factors. Effectiveness factors were calculated in two different approaches: 1) the Thiele modulus approach, and 2) the approach using distributions of concentration and temperature through the porous catalyst pellet. Simulation results of these two models have been compared to the kinetic data obtained by experiments in a packed-bed reactor for verification purpose.

Furthermore, a one-dimensional plug-flow model of a multi-tubular packed-bed reformer with estimation of effectiveness factors for methanol steam reforming over Cu/ZnO/Al₂O₃ catalyst was developed. The intraparticle heat and mass diffusion, heat and mass transfer and pressure drop in catalyst bed along the reactor length, heat transfer in thermal air along the reactor length, heat exchange between the tube side and shell side were considered in this model. Therefore, the performance of the catalytic packed-bed reactor can be predicted under a wide range of operating conditions. Effects of operating temperature and particle size on intraparticle distributions of temperature and concentration have been studied. The profiles of concentration and effectiveness factors for three main reactions along the reactor length have been evaluated. Effects of catalyst particle size on the methanol conversion and pressure drop in catalyst bed have been investigated, and a diameter of 1.5 mm for catalyst particle can be considered as a compromise to maximize the methanol conversion without a large pressure drop. Effects of inlet temperature of thermal air were also studied. Results showed that 400–450°C could be good choice as a compromise temperature of thermal air producing a reasonably high concentration of hydrogen and a low concentration of CO in the produced gas. When choosing the proper hydrogen yield for HT-PEM fuel cells, a higher W/FCH₃OH (ratio of catalyst weight to molar flow rate of methanol), preferably > 264 kg s/mol should be considered to reach a high conversion of methanol.

Experiment

The Cu/ZnO/Al₂O₃ catalyst was prepared and tested in the reactor shown in Figure 40. The reactor was loaded with 3.6553 g of the commercial Cu/ZnO/Al₂O₃ catalyst in the volume of 3.6 mL. Cylindrical catalyst particles with the diameter of 1.5 mm were used. The catalyst was reduced firstly in situ with the volumetric flow rate of hydrogen Q_{H₂} = 0.1 cm³ min⁻¹, and the volumetric flow rate of nitrogen Q_{N₂} = 2 cm³ min⁻¹ for 1 hour. The operating temperature for reduction was controlled in the range of 160-220°C. The reduction reaction rate was

kept low in order to avoid any sintering of catalyst. The reforming process was carried out under the temperature of 220-260°C and the W/FCH₃OH of 44-263 kg s mol⁻¹. The value of S/C was 1.3 since it is considered to be a compromise to maximize the methanol conversion without wasting much energy in water evaporation.

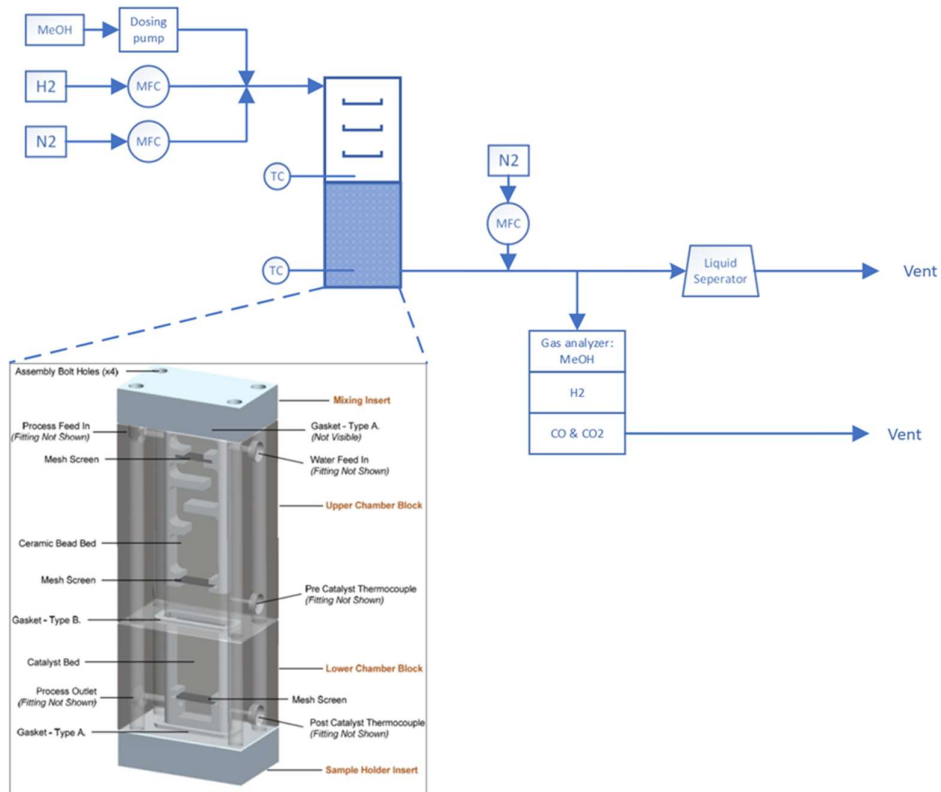


Figure 40: Schematic of the reformer experimental setup

Verification

Three models were developed to investigate the kinetic behavior of the methanol steam reforming process taking into account: 1) kinetic reactions without effectiveness factors, 2) kinetic reactions with an effectiveness factor calculated by Thiele modulus, and 3) kinetic reactions with effectiveness factors calculated by intraparticle distributions of temperature and concentrations. For verification purpose, the simulation results for methanol conversion dependency on the operating temperature and the ratio of the total catalyst mass loaded to the inlet flow rate of methanol (W/FCH₃OH), also known as the contact time, were compared with the experimental data. As shown in Figure 41, a good agreement is shown between the experimental data and the simulation results of the kinetic model with effectiveness factors by distribution approach. So, it can theoretically predict the kinetic behavior of the commercial catalyst.

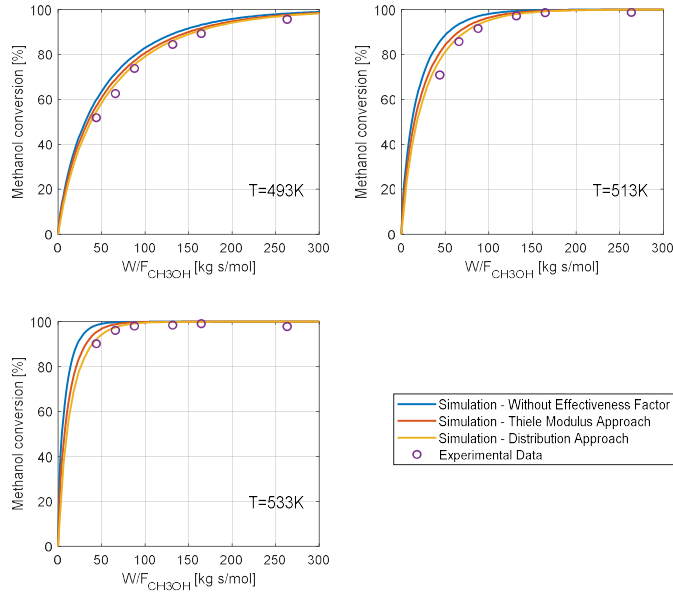


Figure 41: Model verification through comparison of simulation results and experimental data for methanol conversion dependency on operating temperature and contact time

Effects on effectiveness factors

Figure 42 shows the effects of the particle diameter and the bulk flow temperature on the profiles of the temperature drops from the external surface to the center of the pellet at the inlet condition. As can be seen on these figures, the temperature gradients from the center to the surface of the pellet become larger due to the increase of particle diameter and the increase of operating temperature. Owing to the endothermic nature of reforming reactions, a decrease of temperature occurs as the reactions take place inside the pellet. However, heat is supplied from the external surface of the pellet. As the pellet diameter increases, there is an increase in the effect of intraparticle heat transfer limitation; and as the operating temperature increases, reforming reactions taking place inside the catalyst pellet consume a significant amount of heat, which leads to a higher temperature drop inside the catalyst pellet.

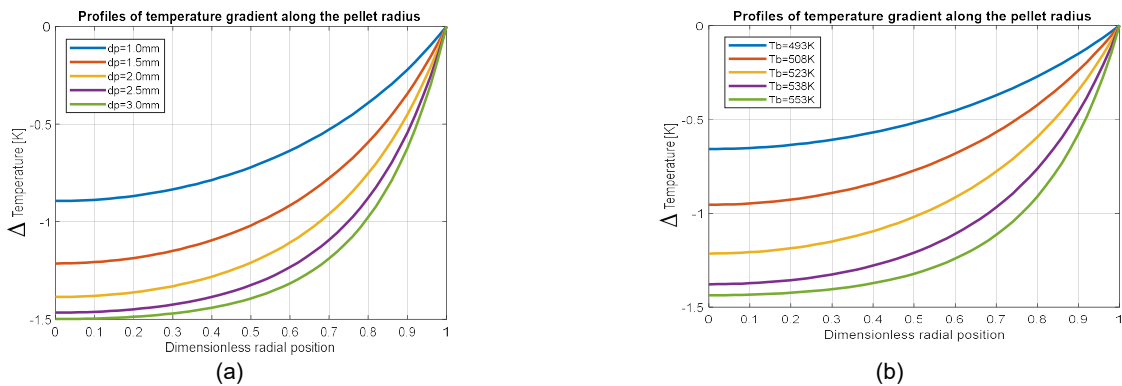


Figure 42: Intraparticle profiles of temperature gradients shown from the pellet centre to the external radius of the pellet at the inlet condition with different (a) diameters of catalyst particle, and (b) temperatures of bulk flow.

Figure 43 shows the profiles of the mole fraction of different components from the pellet center to the external radius of the pellet at the inlet condition with the variation of catalyst size and operating temperature. For a larger diameter of catalyst pellet, there will be a larger gradient of concentration in the radial direction of catalyst pellet due to the diffusion limitation, which leads to a smaller effectiveness factor. When operating under a

higher temperature, the gradient of concentration inside the pellet could be more obvious owing to the diffusion limitation and high reaction rates.

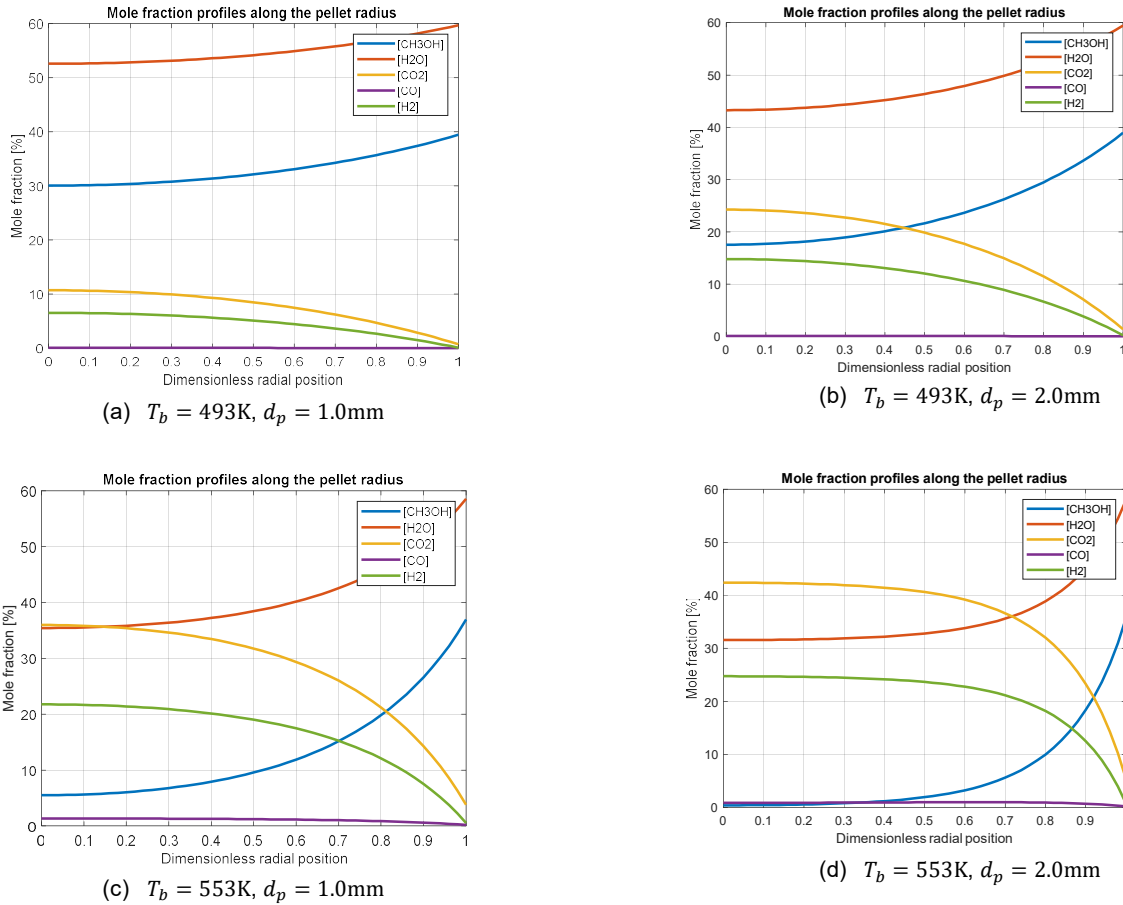


Figure 43: Intraparticle profiles of mole fraction shown from the pellet centre to the external radius of the pellet at the inlet condition with different (a) (b) (c) temperatures and different (d) (e) (f) diameters of catalyst particle

Effects on one-dimensional model

For a multi-tubular packed-bed reactor with the length of 0.48 m, the S/C of 1.5, feed of methanol 4.5 L/hr, inlet temperature of thermal air at 400°C, and inlet temperature of methanol vapor and steam at 160°C, the concentration profiles along the reactor length are shown in Figure 44. And the profiles of effectiveness factor for 3 main reactions along the reactor length are shown in Figure 45.

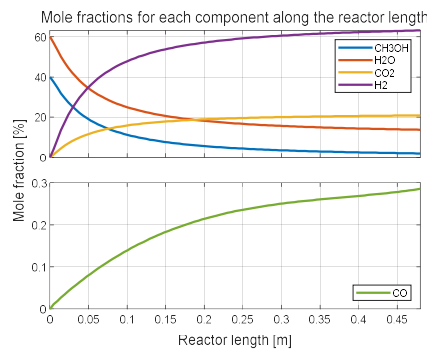


Figure 44: Concentration profiles of concentrations along the reactor length

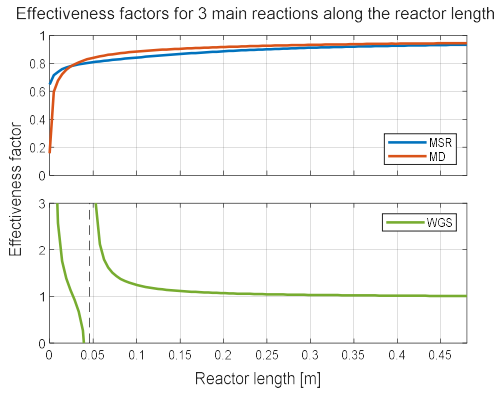


Figure 45: Profiles of effectiveness factors along the reactor length

The effect of catalyst particle size on the methanol conversion and pressure drop along the reactor length are shown in Figure 46. As it shows, the methanol conversion increases with a smaller particle size of catalyst owing to a reduced diffusion limitation inside particle. However, with a smaller particle size, there is a remarkable increase of pressure drop along the reactor length, which is not favored since additional pressure (known as 'pump head') will be needed to accommodate the pressure drop. Therefore, a diameter of 1.5 mm can be chosen as a compromise to maximize the methanol conversion without a large pressure drop.

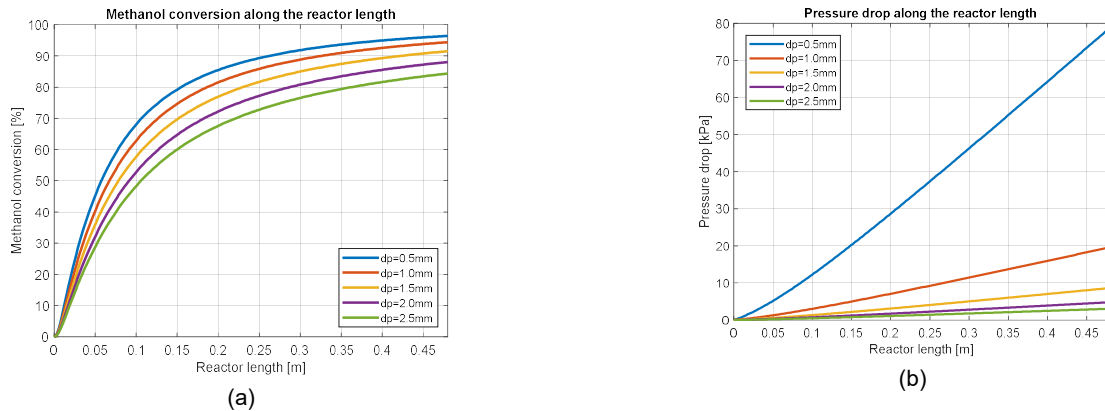


Figure 46: Effects of the diameter of catalyst particles on the distribution of the (a) methanol conversion and (b) pressure drop along the reactor length

Figure 47 (a) reports the effect of inlet temperature of thermal air on the conversion of methanol along the reactor length. As can be seen, the conversion of methanol reaches to 65%, 83%, 96%, 99.7% and 100% when operating with the inlet temperature of thermal air at 300°C, 350°C, 400°C, 450°C and 500°C, respectively. The methanol conversion increases with the increase in inlet feed temperature of thermal air due to the endothermicity of the reforming process of methanol. Figure 47 (b) describes the effect of inlet temperature of thermal on the axial profile of CO concentration in packed bed. The CO concentration in the product gases increase with the increase in the inlet temperature of thermal air. Higher operating temperature in catalyst bed favors the methanol decomposition reaction (MD) and reversed water gas shift reaction (rWGS), which leads to higher production of CO. However, a high concentration of CO in the product should be avoid when feeding into HT-PEM fuel cells. Therefore, 400-450°C is a compromise temperature of thermal air producing a reasonably high concentration of hydrogen and a low concentration of CO in the produced gas.

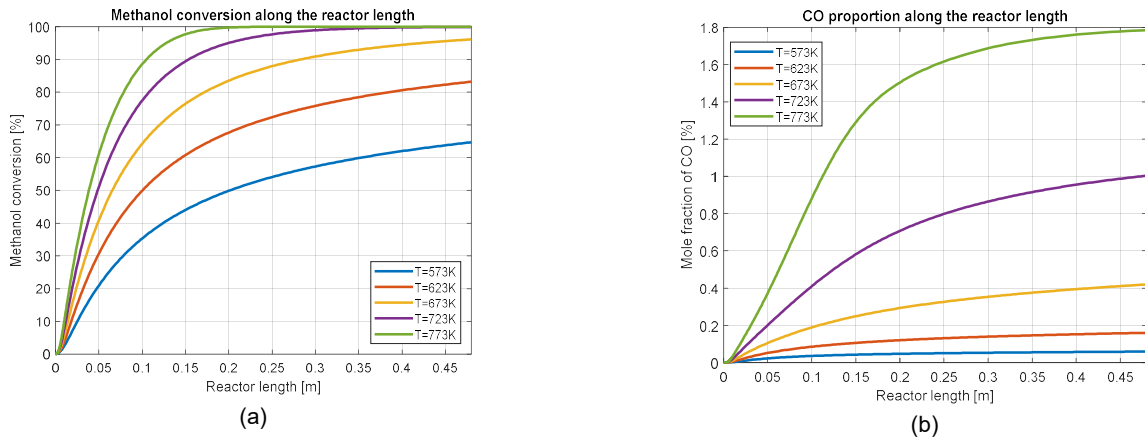


Figure 47: Effects of inlet temperature in thermal air on the distribution of the (a) methanol conversion and (b) CO proportion along the reactor length

Figure 48(a) evaluates the effect of the methanol flow rate on the methanol conversion. The W/FCH₃OH for the methanol feeding rates at 3.0, 3.5, 4.0, 4.5 and 5.0 L/h are 352, 302, 264, 235 and 211 kg s/mol, respectively. The methanol conversion decreases with the increasing methanol flow rate due to the decrease of W/F and higher heat consumption. The profiles of hydrogen yield is shown in Figure 48(b). The yield of hydrogen increases with increasing of methanol flow rate. To have a high hydrogen yield, more methanol should be fed into the reactor. However, to overcome the decrease of methanol conversion caused by increased methanol feed, the inlet temperature of thermal air or the catalyst loading should be increased, which leads to the increased costs. A relatively high methanol conversion could be attained when the W/FCH₃OH is higher than 264 kg s/mol.

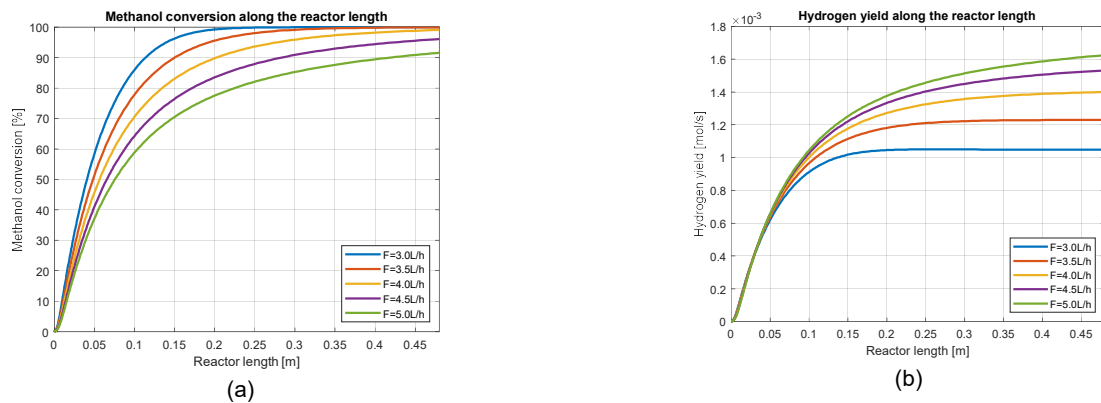


Figure 48: Effects of methanol feeding rate on the distribution of the (a) methanol conversion and (b) hydrogen yield along the reactor length

2D reformer model

To further understand and optimize the methanol steam reformer the 1D model was expanded to 2D model and the two models compared.

To study the effects of radial heat and mass transfer phenomena in the catalyst bed, we developed a 2D model.

Mass and energy balance equations in the tube side:

$$u_s \frac{\partial c_i}{\partial z} = D_{er} \left(\frac{\partial^2 c_i}{\partial r^2} + \frac{1}{r} \frac{\partial c_i}{\partial r} \right) + \eta_i \rho_c r_i$$

$$u_s \rho_f C_{p,f} \frac{\partial T_t}{\partial z} = \lambda_{er} \left(\frac{\partial^2 T_t}{\partial r^2} + \frac{1}{r} \frac{\partial T_t}{\partial r} \right) + \sum \eta_j \rho_c (-\Delta H_j) r_j S_c$$

Boundary conditions:

$$\begin{aligned}
 c = c_0, T = T_0 & & z = 0, 0 \leq r \leq R_t \\
 \frac{\partial c}{\partial r} = 0 & & r = 0 \text{ and } r = R_t \\
 \frac{\partial T}{\partial r} = 0 & & r = 0, \text{ all } z \\
 \frac{\partial T}{\partial r} = -\frac{U_t}{\lambda_{er}}(T - T_s) & & r = R_t
 \end{aligned}$$

Comparison between 1D and 2D model

By using the 2D model, we can study the temperature and concentration gradients in both axial direction and radial direction in the catalyst bed.

1. Effect of the inlet temperature of burner gas is shown in Figure 49.

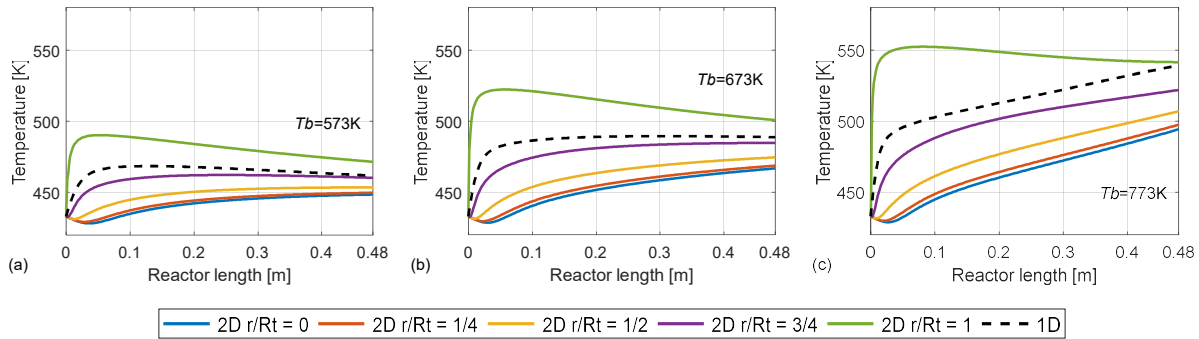


Figure 49: Effect of the inlet temperature of burner gas T_b on axial temperature profiles at different radial positions (r/R_t): $D_t = 32.6 \text{ mm}$, $W_{catalyst}/F_{CH_3OH} = 135 \text{ kg s mol}^{-1}$

When we increase the inlet temperature of burner gas, the temperature gradients from the tube wall to the centre of the reactor tube (radial temperature gradients) will be increased. It also leads to an increase of the hot spot temperature, which should be avoid in case of the thermal sintering of catalysts.

2. Effect of the contact time is shown in Figure 50.

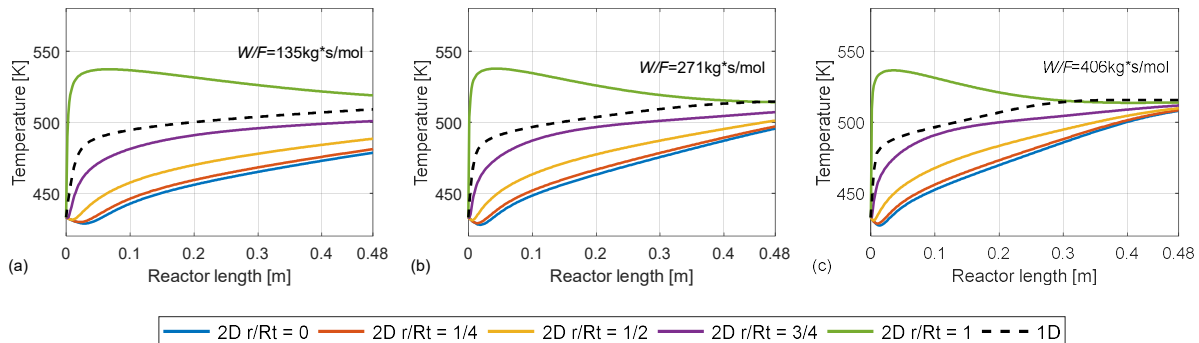


Figure 50: Effect of the $W_{catalyst}/F_{CH_3OH}$ on axial temperature profiles at different radial positions (r/R_t): $D_t = 32.6 \text{ mm}$, $T_b = 723 \text{ K}$

When we have a large value of $W_{catalyst}/F_{CH_3OH}$, which means a small flow rate of methanol F_{CH_3OH} , less energy will be consumed in the catalyst bed. Therefore, temperature can be more uniformly distributed in the radial direction near the outlet of the reformer.

3. Effect of the tube diameter is shown in Figure 51.

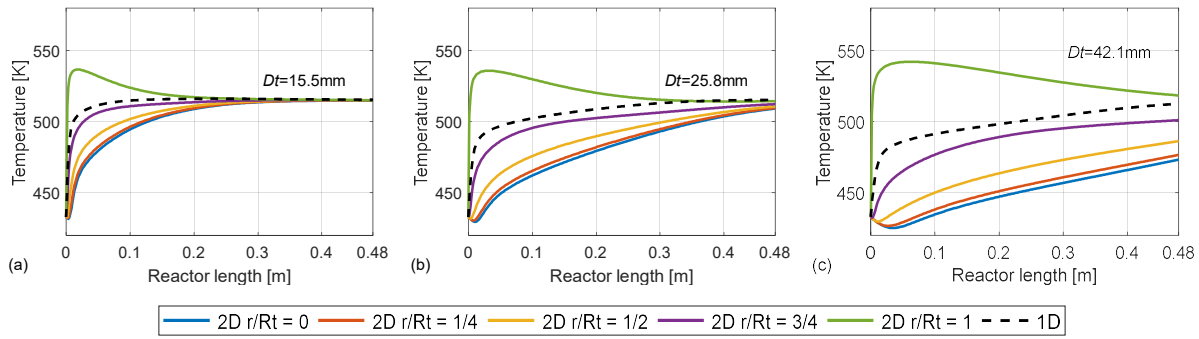


Figure 51: Effect of the tube diameter D_t on axial temperature profiles at different radial positions (r/R_t): $T_b = 723\text{ K}$, $W_{catalyst}/F_{CH_3OH} = 271\text{ kg s mol}^{-1}$

As shown in Figure 52, decrease in the tube diameter will significantly reduce the radial temperature gradients, and lead to a more efficient heat transfer and more uniformly distributed temperature in the catalyst bed.

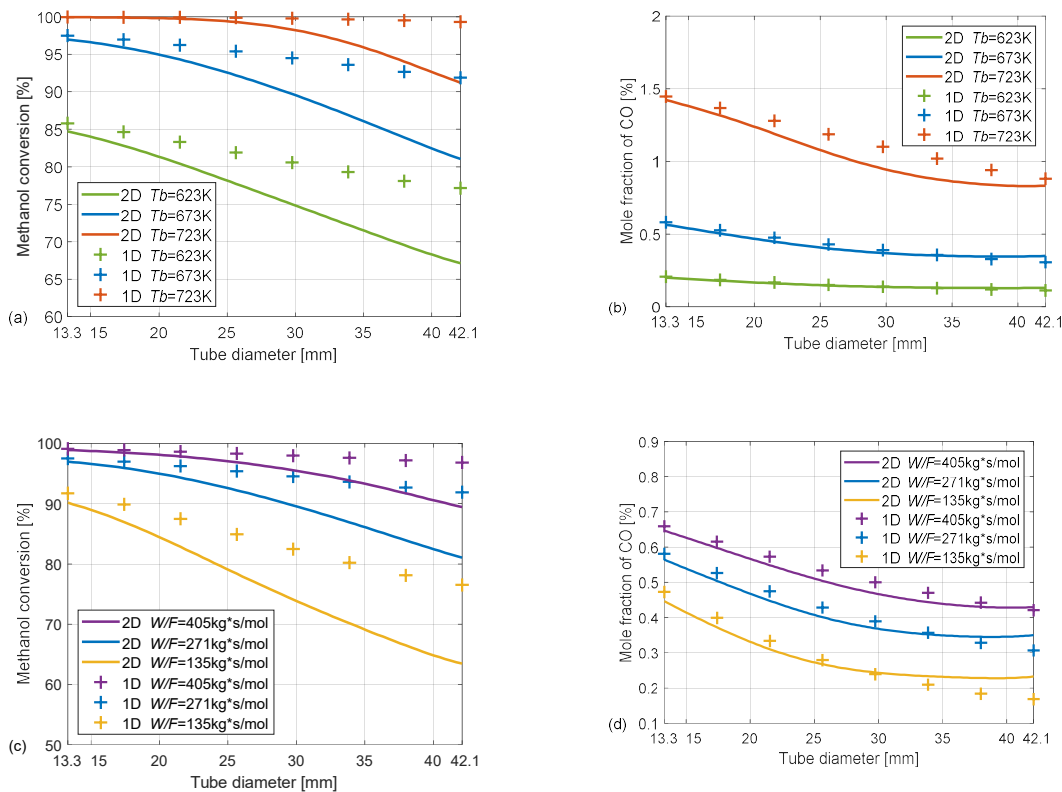


Figure 52: Effect of the tube diameter D_t and the inlet temperature of burner gas T_b on axial profiles of (a) the methanol conversion, and (b) the mole fraction of CO: $W_{catalyst}/F_{CH_3OH} = 271\text{ kg s mol}^{-1}$, effect of the tube diameter D_t and the $W_{catalyst}/F_{CH_3OH}$ on axial profiles of (c) the methanol conversion, and (d) the mole fraction of CO: $T_b = 673\text{ K}$

With the increase of the inlet temperature of burner gas T_b , and the increase of contact time $W_{catalyst}/F_{CH_3OH}$, the methanol conversion and the CO concentration in the reformat gas are increased. This is because the increase in the burner temperature enhanced the temperature in the catalyst bed. This elevated temperature favors the MSR reaction so that the methanol conversion is increased. Moreover, the increase temperature also favors the re-WGS reaction and MD reaction. Hence, more CO is produced during the reforming process. The increased $W_{catalyst}/F_{CH_3OH}$ will leads to an increased and more uniformly distributed temperature in the catalyst bed, so that it improves the methanol conversion of the reformer.

By comparing the difference between the 1D and 2D models, we can tell if the radial gradients in the catalyst bed significantly affect the performance of the reformer. This comparison is shown in Figure 52, and it can be concluded that for smaller tube diameter ($< 15\text{ mm}$), the simpler 1D model can be used to simulate the reformer

performance instead of the 2D model without sacrificing much accuracy. And by using the 2D model, we could do the multi-objective optimization for improving the reformer design.

Dynamic model of the methanol steam reformer

To study the transient behavior of the multi-tubular packed-bed reactor, we developed a 1D dynamic model.

Mass and energy balance equations in the tube side:

$$\varepsilon \frac{\partial C_i}{\partial t} = -u_s \frac{\partial C_i}{\partial z} + \frac{\partial}{\partial z} \left(D_{ez} \frac{\partial C_i}{\partial z} \right) - R_i(C, T)$$

$$(\varepsilon \rho_f c_{p,f} + (1 - \varepsilon) \rho_s c_{p,s}) \frac{\partial T}{\partial t} = -u_s \rho_f c_p \frac{\partial T}{\partial z} + \frac{\partial}{\partial z} \left(\lambda_{ez} \frac{\partial T}{\partial z} \right) + R_T(C, T) - \frac{4U_w}{d_t} (T - T_w)$$

Boundary conditions:

$$t = 0 \quad C_i = C_i^0, T = T^0$$

$$z = 0 \quad u_s C_{i,0} = u_s C_i - D_{ez} \frac{\partial C_i}{\partial z}$$

$$u_s \rho_f c_p T_0 = u_s \rho_f c_p T - \lambda_{ez} \frac{\partial T}{\partial z}$$

$$z = L \quad \frac{\partial C_i}{\partial z} = 0$$

$$\frac{\partial T}{\partial z} = 0$$

Simulation results of the dynamic model

First, preheat the reformer from ambient temperature to 160°C. After that, several steps are taken:

1. Increase the inlet temperature of burner gas $T_{b,0}$ from 160°C to 400°C, shown in Figure 53.

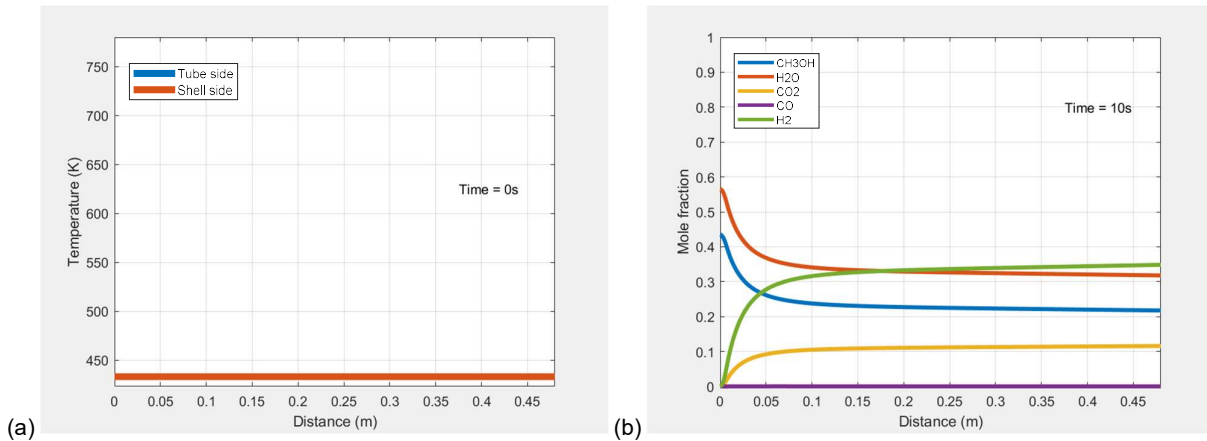


Figure 53: Profiles of (a) temperature in both tube and shell sides and (b) mole fraction of different components along the reactor length at various time points: inlet temperature of reactants $T_0 = 160^\circ\text{C}$, inlet flow rate of methanol $F_{CH_3OH} = 4.5 \text{ L/h}$

When we increase the inlet temperature of burner gas to 400°C and start feeding the methanol and water mixture into the catalyst bed, temperatures in both tube side and shell side are increased during the heat exchanging process. More methanol will also be reacted during this process.

2. Increase the inlet temperature of burner gas $T_{b,0}$ from 400°C to 500°C, shown in Figure 54.

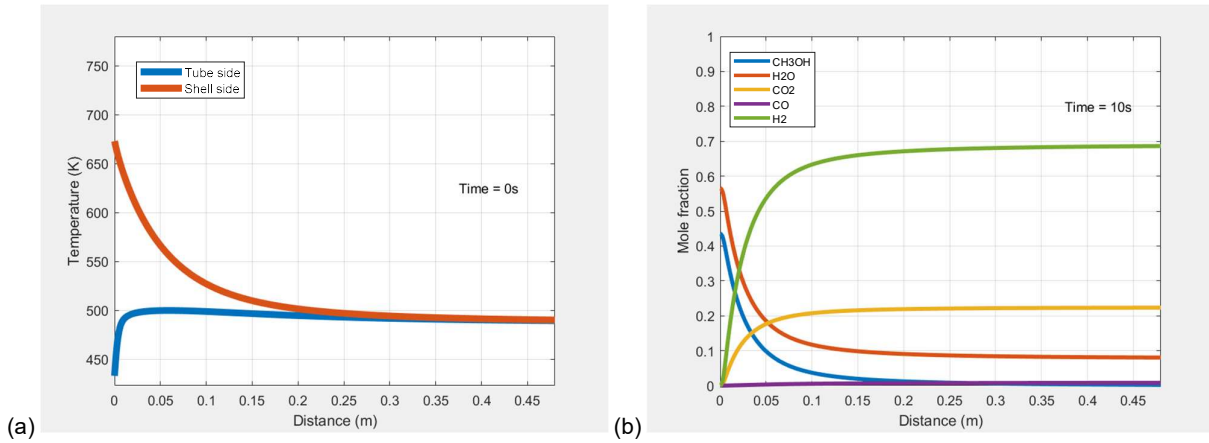


Figure 54: Profiles of (a) temperature in both tube and shell sides and (b) mole fraction of different components along the reactor length at various time points: inlet temperature of reactants $T_0 = 160^\circ\text{C}$, inlet flow rate of methanol $F_{\text{CH}_3\text{OH}} = 4.5 \text{ L/h}$

Moreover, we can study the transient behavior of the reformer when we change the burner temperature from 400°C to 500°C . When we change the burner temperature, the temperatures in both tube and shell sides are gradually increased until the steady state is achieved.

Increase the flow rate of methanol $F_{\text{CH}_3\text{OH}}$ from 4.5 L/h to 6.75 L/h , shown in Figure 55.

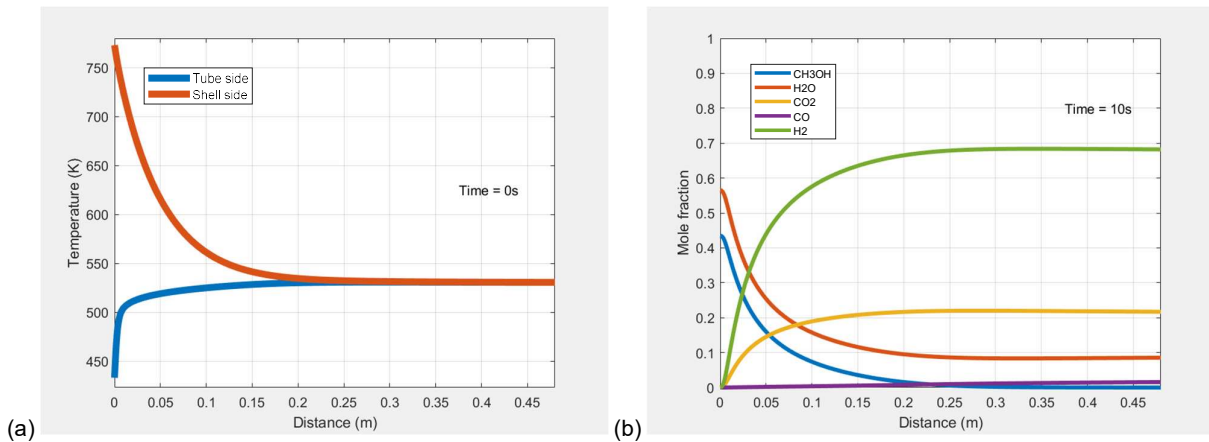


Figure 55: Profiles of (a) temperature in both tube and shell sides and (b) mole fraction of different components along the reactor length at various time points: inlet temperature of reactants $T_0 = 160^\circ\text{C}$, inlet temperature of burner gas $T_{b,0} = 500^\circ\text{C}$

We can also study the transient behavior when we change the fuel feeding rate. As we can see, when we increase the flow rate of methanol from 4.5 L/h to 6.75 L/h (with $\text{S/C} = 1.3$), the temperatures in both tube and shell sides are decreased because more energy is consumed in the catalyst bed. The hydrogen concentration in the reformat gas is slightly reduced.

By using the dynamic model, we can further study and optimize the start-up process to minimize the start-up time, eliminate the CO concentration in the reformat gas, and realize high efficiency and stable operation of the reformer.

Work package 7: System Performance

- The realized performance of the new Serene U-5 G4 fuel cell unit is included in Table 7: Performance of the Serene U-5 G4 fuel cell unit:

Table 7: Performance of the Serene U-5 G4 fuel cell unit

PERFORMANCE	
Max power output ¹ [kW]	5
Nominal output [kW]	3.75
Output Voltage ² [Vdc]	42 - 58
Power turndown [%]	0 - 100
IP rating	IP-20

1. Max power at beginning of life

All numbers related to kW or kWh is electrical power / Energy delivered at unit terminals (kWe / kWh_e)

2. Contact SerEnergy for other voltage variants.

- Work is ongoing regarding finishing a high voltage variant for the fuel cell unit, addressing other markets than the 48VDC (which is the typical telecom base station usage the unit are targeting). The realized physical and geometrical dimensions of the Serene U-5 G4 fuel cell unit can be seen in Table 8: Overall dimensional specifications of the Serene U-5 G4 fuel cell unit:

Table 8: Overall dimensional specifications of the Serene U-5 G4 fuel cell unit

WEIGHT & DIMENSIONS	
Hight [mm]	300
Width [mm]	495
Length ⁴ [mm]	852
Weight [kg]	77
Volume [l]	126,5

4. Length excluding handles, connectors on front and exhaust pipes on rear

- Regarding operation of the new realized fuel cell unit, a few additional details are listed in Table 9: Operation specifications for the Serene U-5 G4 module:

Table 9: Operation specifications for the Serene U-5 G4 module

OPERATIONS	
Fuel mix	60% vol methanol, 40% vol deionized water
Fuel consumption ³ [l/kWh]	0,9
Net electric efficiency ³ [%]	41
Ambient temperature [°C]	-20°C and up to 50°C
Interfaces	GPIO, HTTP/SNMP/Ethernet IP, CANopen, USB

3. At beginning of life and nominal load

A manual of the certified product is available for customers with further details of specifications

Work package 8: Box Development & Build

A product development strategy used for managing a new prototype system has been utilized in order to ensure proper communications, risk management and efficiency in execution. This is known as the product life cycle, and it has been visualized in Figure 56.

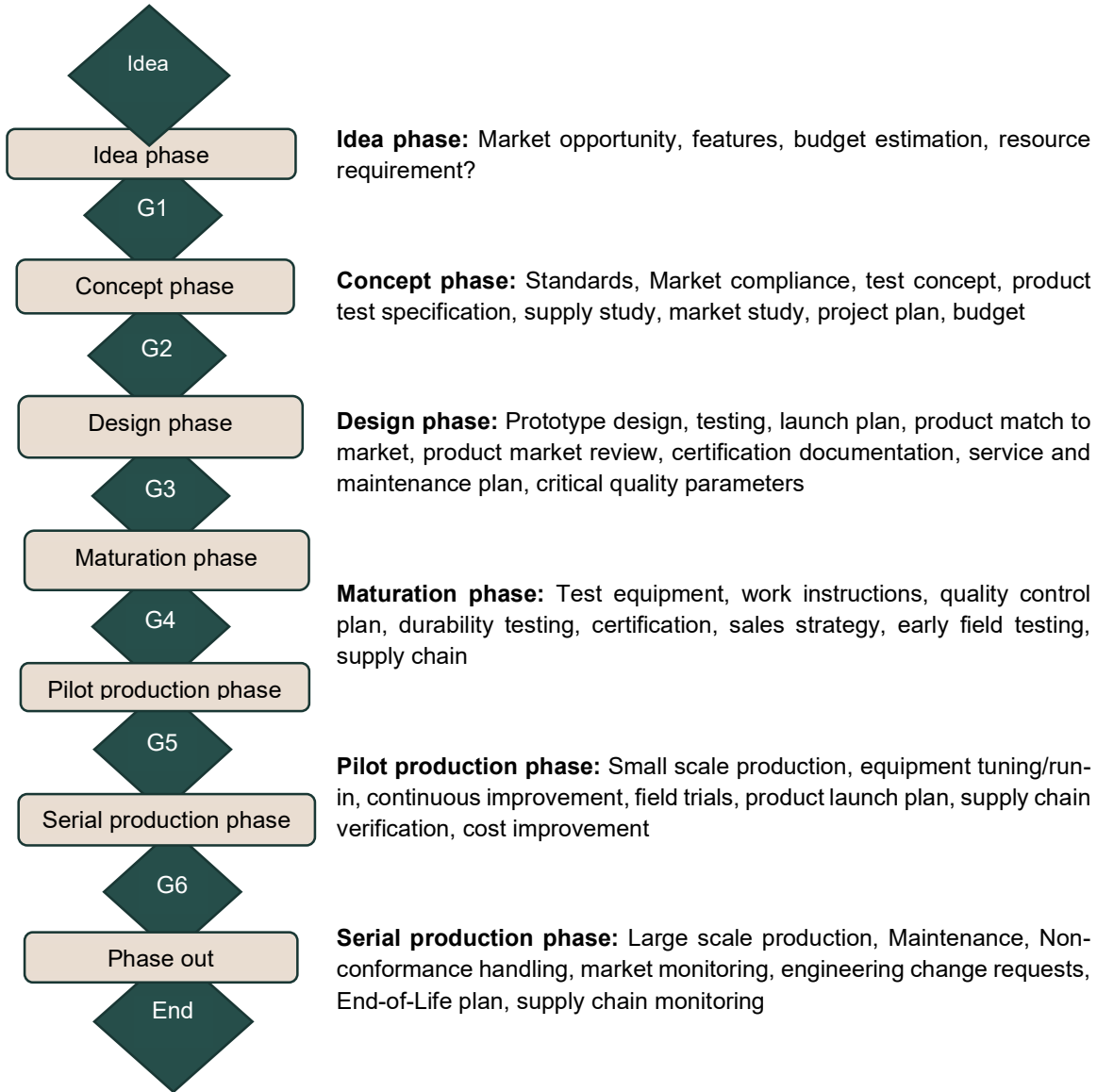


Figure 56: Summary of product life cycle development strategy

In the figure above, each of the different diamond shaped boxes represent a gate meeting, a certain set of requirements needed to be fulfilled before moving through to the next phase of the product life cycle. Each phase (square box) includes various activities, each important to complete in order to efficiently to be able to execute the product development plan, production and product launch as planned. The Serene U-5 G4 is current preparing for its pilot production phase.

Laboratory tests were made on a hybridized system with batteries (72V 50Ah), with small load testing up to 1 - 5kW; to move to the next step, additional batteries would be required (72V 100Ah) for the vehicle to perform more detailed road test. The fuel cell module can output a stable power up to ~3000W with the mounted prototype fuel cell stack, and the stack voltage will then start to level out after the I_{FC} current ramping up over 58A.

The exhaust temperature has also been tested, the high side showing about 53 degrees C, demonstrating that cooling was okay and under control. The developed vehicle enclosure has shown good protection for vibrations and rain drops as there are 5 springs at the bottom and sealed with EVA foam.

The module is currently too large to fit under the vehicle, therefore it is installed on the top. The plan would be to integrate it as part of the chassis.

Battery and fuel tank installations are planned on the on the sides of the vehicle.



Figure 57: Fuel cell installed on vehicle

Work package 9: Box Concept Controls.

To optimize control strategies for the reformed methanol fuel cell-based hybrid (+Battery) power train for automotive application a complete system model is being developed. A schematic of the components of the model are shown in Figure 58. The battery acts as a buffer to supply the peak loads and can also be used to provide power to the reformed methanol fuel cell system during start-up.

It was concluded that, the operating temperature range between 160°C and 170°C can be considered optimal, as illustrated in the figure below. There is a significant increase in performance compared to lower operating temperatures without too much penalty in terms of lifetime like the higher operating temperatures (> 180°C).

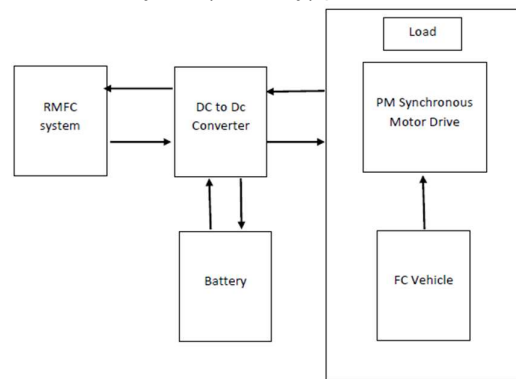


Figure 58: An RMFC system combined with a battery in a hybrid system for vehicle power train.

More details regarding this are available in some of the referred work from Aalborg University

On system level the, Figure 59 shows a screen grab from one of the running SereneU units in an operational situation, where the unit is delivery clean power from a methanol fuel source. The interface is able to provide a detailed overview of the different system states, visualizing currents, voltages, temperatures, pressures, rotational speeds and duty cycles. The interface also permits configuration of the desired battery charging and control conditions in the hybrid electrical system. Thus, the fuel cell charging unit can be used in several types of installations, including vehicles on land sea and in the air; and stationary applications in remote areas.

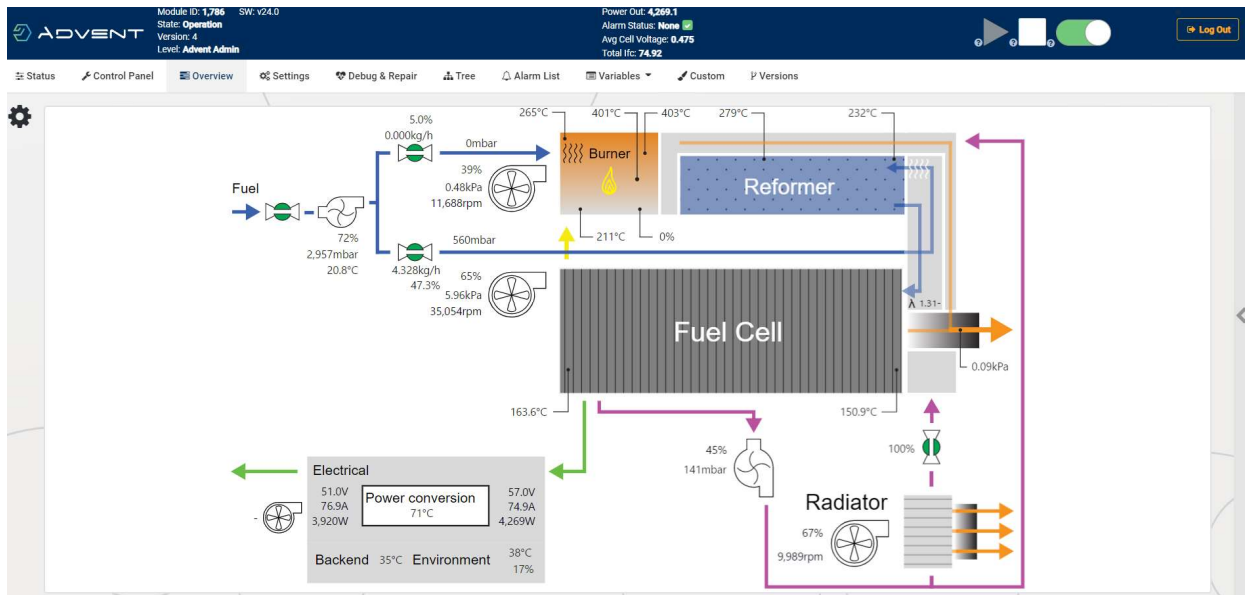


Figure 59: Graphical user interface from a running SereneU unit

Work package 10: Commercial Compliance.

A SereneU unit has been constructed with a prototype stack with Dapozol MEAs. The unit needed to differ a bit from the standard 48VDC unit produced in Aalborg. Instead, it needs to be able to handle a 72VDC bus for the small electric demonstration vehicle.

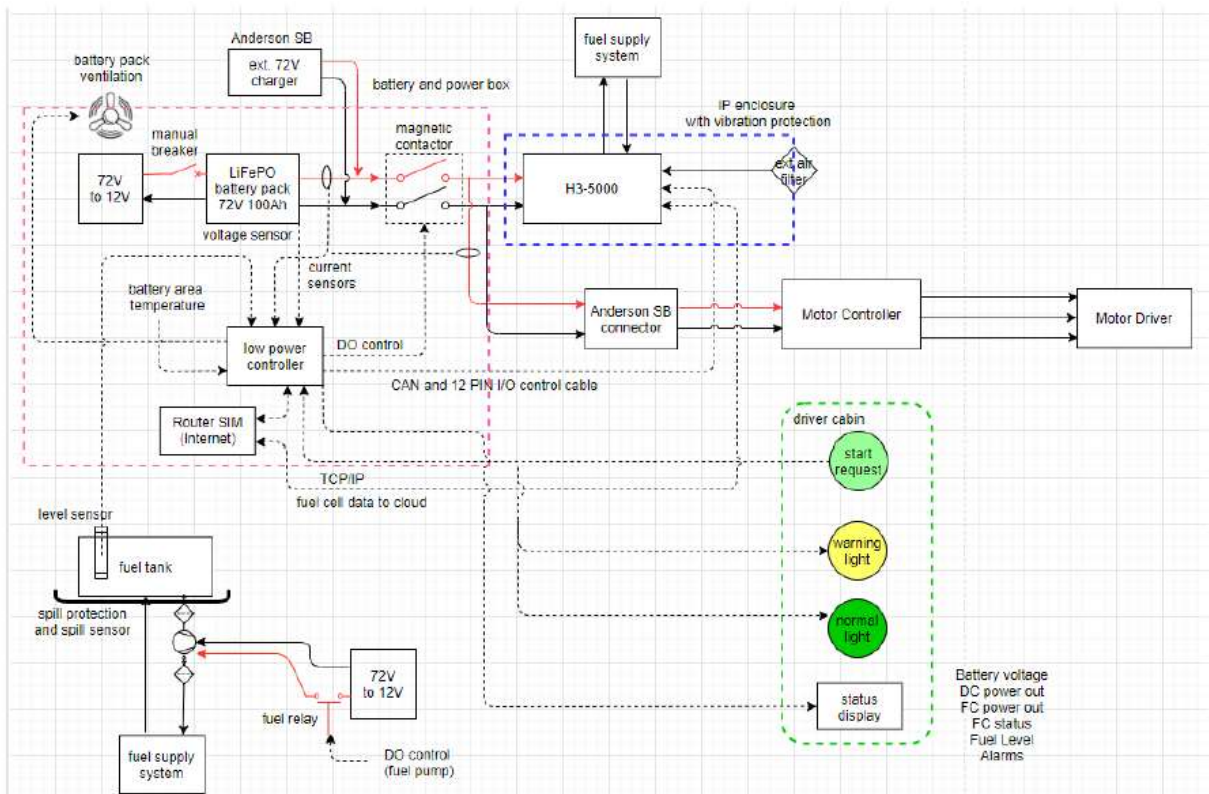


Figure 60: Diagram of the electric vehicle power train (H3-5000 shows the draft position of the SereneU system)

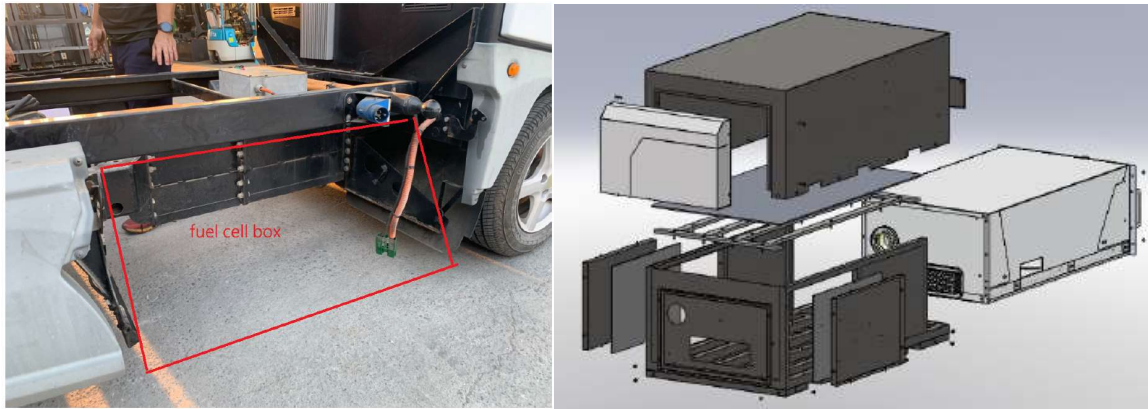


Figure 61: Left, picture of space for the fuel cell box

Right, Climate box to ensure unit is protected from weather

Work on the prototype was delayed multiple times due to various circumstances, however as illustrated in WP8, a prototype has been built and is operational, although it did not get much time to test durability of the system in a road context. This however was possible in a parallel customer engineering activity; this is mentioned later in “4. Project implementation”.

Work package 11: Dissemination

The project dissemination occurred through several conference participations and a strong line of peer-reviewed journal publications listed in the following:

M Zhou, S Frensch, V Liso, N Li, SL Sahlin, G Cinti, S Simon Araya, *Modeling the Performance Degradation of a High-Temperature PEM Fuel Cell*, *Energies* 15 (15), 5651

J Zhu, X Cui, SS Araya, *Comparison between 1D and 2D numerical models of a multi-tubular packed-bed reactor for methanol steam reforming*, *International Journal of Hydrogen Energy*

J Zhu, SS Araya, X Cui, SK Kær, *The role of effectiveness factor on the modeling of methanol steam reforming over CuO/ZnO/Al₂O₃ catalyst in a multi-tubular reactor*, *International Journal of Hydrogen Energy* 47 (14), 8700-8715

SS Araya, N Li, V Liso, *Degradation and failure modes in proton exchange membrane fuel cells*, Book chapter in *PEM Fuel Cells*, 199-222

David Batet, Fatema T. Zohra, Simon B. Kristensen, Søren J. Andreasen, Lars Diekhöner, *Continuous durability study of a high temperature polymer electrolyte membrane fuel cell stack*, *Applied Energy*, 2020, vol 277

S Simon Araya, S Thomas, A Lotrič, S Lennart Sahlin, V Liso, *Effects of impurities on pre-doped and post-doped membranes for high temperature PEM fuel cell stacks*, *Energies* 14 (11), 2994

J Zhu, SS Araya, X Cui, SL Sahlin, SK Kær, *Modeling and design of a multi-tubular packed-bed reactor for methanol steam reforming over a Cu/ZnO/Al₂O₃ catalyst*, *Energies* 13 (3), 610

SS Araya, V Liso, X Cui, N Li, J Zhu, SL Sahlin, SH Jensen, MP Nielsen, *A Review of The Methanol Economy: The Fuel Cell Route*, *Energies* 13 (3), 596

Y. Hu, J. O. Jensen, P. Bretzler, L. N. Cleemann, J. Yu, Q. Li, *Revealing the genuine stability of the reference Pt/C electrocatalyst toward the ORR*, *Electrochimica Acta*, 391 (2021), 138963

D. Aili, D. Henkensmeier, S. Martin, B. Singh, Y. Hu, J. O. Jensen, L. N. Cleemann, Q. Li, *Polybenzimidazole-Based High-Temperature Polymer Electrolyte Membrane Fuel Cells: New Insights and Recent Progress*, *Electrochemical Energy Reviews* 3 (2020), 793–845

D. Aili, J. Yang, K. Jankova, D. Henkensmeier and Q. Li, *From polybenzimidazoles to polybenzimidazoliums and polybenzimidazolides*, J. Mater. Chem. 8A (2020), 12854

J. Zhang, D. Aili, S. Lu, Q. Li, and S. P. Jiang, *Advancement toward Polymer Electrolyte Membrane Fuel Cells at Elevated Temperatures*, Research, 2020, 9089405

H. Tang, D. Aili, K. Geng, J. Gao, Q. Li, N. Li, *On the stability of imidazolium and benzimidazolium salts in phosphoric acid-based fuel cell electrolytes*, Journal of Power Sources, 515(2021), 230642

Y. Chen, K. Azizi, W. Zhang, D. Aili, S. Primdahl, L. N. Cleemann, H. A. Hjuler, Q. Li, *Feasibility of using thin polybenzimidazole electrolytes in high-temperature proton exchange membrane fuel cells*, Inter. J. Hydrogen Energy, 47 (2022), 28615-28625

Q. Zhou, J. O. Jensen, L. N. Cleemann, Q. Li, *Tailoring the particle sizes of Pt5Ce alloy nanoparticles for the oxygen reduction reaction, submitted to Advanced Sensor and Energy Materials* (May 2022, ASEMS-D-22-00030)

Several conference presentations from DTU, BWT and Advent at *HiPEM Tech 2022 – Workshop on High Temperature polymer electrolyte membrane fuel cell technology – Materials and Applications*, 22nd-24th June 2022, Bad Zwischenahn, Germany

- *Which energy technology has been developed and demonstrated?*

An optimized fuel cell application has been developed, to specifically satisfy demand in the light commercial vehicle industry. The developed fuel cell enables similar vehicle characteristics to traditional internal combustion engine vehicles. Internal production processes have also been developed and optimized, thus reducing overall costs of fuel cell applications, while simultaneously reducing material waste. Furthermore, new materials have been tested and implemented in the product, to reduced overall cost and increase the product lifetime.

4. Project implementation

- *Did the project experience problems not expected?*

The project was affected by external circumstances, i.e., the global Covid pandemic hindered some aspects of the project, as participants were incapable of traveling and forced to work from home to some extent. This complicated matters and made it difficult to achieve the desired level of collaboration between partners. However, virtual collaboration was maintained throughout the project i.e., meetings, brainstorming, etc., took place on digital platforms throughout the project timeline, and critical laboratory and manufacturing activities were also possible to keep active during the troublesome period.

Serenergy A/S (now Advent Technologies A/S) and Danish Power Systems (now Blue World Technologies) were both acquired by external companies during the project period. This led to a restructuring and reorganization of the two companies, which changed internal organizational prioritization and ambitions, therefore also affecting the project in agreement with EUDP.

- *How did the project evolve?*

A high degree of collaboration was maintained throughout the project, even though external circumstance made working conditions suboptimal. Objectives and milestones were mostly achieved, however some WPs were delayed and rescope in order to complete them within the project framework. This naturally also affected the end stage of the project and ability to properly integrate some of the developed technologies into a running vehicle prototype. To make up for this, additional time was spent on additional non-vehicle demonstration activities, showing the durability of the developed technologies.

- *Describe the risks associated with conducting the project.*

Some of the initially described risks of the project were avoided and navigated successfully. However, since initiating this project public- and policymakers' preference and attention has increased away from light commercial vehicles, and more towards heavy duty and marine activities, where the market demands are more apparent.

- *Did the project implementation develop as foreseen and according to milestones agreed upon?*

As mentioned previously, the entire project was affected by external circumstance, which lead to a restructuring of involved participants and the project in general. Milestones were completed successfully, and overall objectives of the project was still realised. However, the collaboration was incapable of proceeding as planned, mainly due to restrictions enforced by the Covid pandemic. This prevented the close level of cooperation between participants, which was expected and agreed upon, during original planning of the project.

The prototype unfortunately remains incomplete, as installations and design have not been successfully implemented yet. It remains a priority among involved participants to complete the vehicle, as this is essential to be able to publicise material and market the application. However, several customers at Advent Technologies A/S showed interest in similar applications, and the technology has been demonstrated to a large extent in customer projects on vehicle level. A great example of this is ARM engineering showing a record breaking performance of more than 2000km, with an Advent 5kW HTPEM fuel cell system as a range extender. Even though this demonstration does not include all components developed in the COBRADrive project; a significant amount of the experiences gained in the project were instrumental to this successful demonstration.



Figure 62: Breaking records! Electric Renault Zoe running 2000km before requiring charging. Using Advent 5kW HTPEM fuel cell system.

Link to press release: <https://ir.advent.energy/news/news-details/2022/Advents-Methanol-Based-Fuel-Cell-Unit-Contributes-to-a-New-World-Record-set-by-ARM-Engineering-for-Both-Electric-and-Hydrogen-Powered-Cars/default.aspx>

5. Project results

- *Was the original objective of the project obtained? If not, explain which obstacles that caused it and which changes that were made to project plan to mitigate the obstacles.*

As mentioned in the previous section, external circumstances caused some issues during the project. However, during these times, the project participants continued the collaboration using various online tools to communicate and solve objectives. It would have been preferable to assist each other by being physically present, however, the participants managed to make it work, mitigating problems, rescoping internal projects to still meet deadlines and solve unforeseen problems and delays.

- *Describe the obtained technological results. Did the project produce results not expected?*

The main technological outcome includes production level results on realized and efficient, low-cost manufacturing at Blue World Technologies when it comes to membrane and electrode manufacturing. Furthermore, the revision of the SereneU 5kW HTPEM fuel cell unit was also completed and successfully put into production. More in-situ demonstration in the planned vehicle was expected, but the pandemic situation and logistic crisis reduced some of the possibilities; however, a parallel customer activity, equally demonstrated the capabilities of the developed technologies.

- *Describe the obtained commercial results. Did the project produce results not expected?*

Large scale MEA production was a great commercial success at Blue World Technologies, and the development of a commercially compliant fuel cell unit at Advent was a good success as well, with multiple units sold before project finalization.

- *Target group and added value for users: Who should the solutions/technologies be sold to (target group)? Describe for each solutions/technology if several.*

The targeted customer group of the project was primarily light commercial vehicles, to increase the range and capacity of battery powered light commercial vehicles. The capacity of batteries limits its market-potential in applications where heavy loading- and long driving range is essential. A fuel cell powered vehicle is capable of complying with these performance requirements, while simultaneously being CO₂-neutral. Furthermore, refuelling times is similar to traditional vehicles, thus allowing operators of light commercial vehicles to have similar autonomy, flexibility, and loading capacity as in traditional vehicles.

The application developed in the project, also provides a possibility of marketing the application to other markets, with similar requirements and low level of competing applications, e.g., medium-duty, vehicles, heavy-duty vehicles, busses, etc. These sectors are experiencing similar issues to light commercial vehicles, as they require a substitutional application to the traditional internal combustion engine, especially those vehicles that is used for long distance driving. As mentioned previously, battery-powered vehicles are the best option in some cases, i.e., vehicles with short traveling time e.g., urban shipping, that stand idle during night-time, thus capable of re-charging. However, if there are significant requirements to large loading capacity, large traveling distances, etc., then fuel cell applications could be a better fit than batteries. Similarly, if the vehicle is required to operate 24/7 in shifts by different drivers, then batteries are unfit, due to long recharging times.

Another important aspect is the required infrastructure. Battery-powered applications requires significant investments in a large charging infrastructure and innovative charging capabilities, to reduce current recharging times. Introducing a hydrogen gaseous infrastructure, for LTPEM fuel cell vehicles, would be even more costly and resource consuming, due to unwieldiness of hydrogen in both storage and transport.

The fuel cell application in this project requires methanol and as previously stated, this is already being shipped in large scale globally. Furthermore, the existing refuelling infrastructure can be repurposed to store and supply methanol instead of fossil fuel, thus, this solution significantly reduces the required investment and resources needed to implement it.

- *Where and how have the project results been disseminated? Specify which conferences, journals, etc. where the project has been disseminated.*

Please visit the section “Work package 11: Dissemination”

6. Utilisation of project results

- *Describe how the obtained technological results will be utilised in the future and by whom*

This project has enabled Advent Technologies A/S to enter the mobility industry, instead of only focussing on stationary product in a significantly smaller and limited market. The mobility industry provides considerable opportunities to generate revenue and jobs, at a much larger scale than stationary products. Furthermore, this industry requires substitutional applications, due to emissions regulations enforced on traditional vehicles and eventual phaseout, while battery-powered applications are incapable of providing the level of flexibility, range, loading capacity, etc., that is required. This project provides an alternative application which is CO₂-neutral, while maintaining performance characteristics of traditional vehicles.

Blue World Technologies has successfully streamlined its internal production processes and reduced waste materials. Furthermore, Blue World Technologies has reduced the amount of material used in the process, while simultaneously optimizing and bettering the product.

- *Describe how the obtained commercial results will be utilised in the future and by whom the results will be commercialised.*
 - *Did the project so far lead to increased turnover, exports, employment and additional private investments? Do the project partners expect that the project results in increased turnover, exports, employment and additional private investments?*

Advent Technologies A/S have initiated collaborations with various vehicle manufacturers to introduce the application to the industry, as there is an industry-wide expectancy that fuel cell applications will supplement battery applications. It is expected that battery applications will dominate short haul vehicles, whereas fuel cell powered vehicles will dominate the market for long haul vehicles with large capacity requirements.

The results of this project will be utilized to show potential partners/customers the capabilities and the potential of fuel cell powered vehicles. There is an internal expectancy that the mobility industry will be the primary market going forward and the level of interest will increase rapidly, when these industries are subject to large emission fines and forced to implement zero emission vehicles.

- *Describe the competitive situation in the market you expect to enter.*
 - *Are there competing solutions on the market? Specify who the main competitors are and describe their solutions.*

The competing solutions in light commercial vehicles, is mainly battery electric vehicles and traditional vehicles. However, Low Temperature PEM (LTPEM) fuel cell vehicles also competes for market share.

- Battery electric vehicles: These vehicles have severe capacity constraints in both range and loading capacity. Recharging times is another constraint and the more capacity the vehicle has, the longer the recharging times is.
- Traditional internal combustion engine vehicles: This type of vehicle will be phased out eventually, due to global climate regulations and objectives. Furthermore, the current vehicle fleet will be imposed regulations and fines in accordance with pollutions they emit, thus eventually transitioning the entire vehicle fleet to zero emission vehicles.
- LTPEM fuel cell vehicles: The infrastructure required to refuel these vehicles is very costly, as the fuel must be high purity gas, not a liquid. Furthermore, LTPEM fuel cells suffers from issues relating to e.g.,

heating management, low CO tolerance, low system efficiency, etc., thus making them unfit for the vehicle industry.

The competitive advantages of the application in this project, is of course the CO₂-neutrality, but also its ability to compete with traditional vehicles on essential performance objectives, e.g., range, capacity, etc. Furthermore, it also reduces the substantial cost of implementing the necessary infrastructure in alternatives, i.e., hydrogen gas or electric charging, as the pre-existing infrastructure can be reused and repurposed to supplying green methanol instead of traditional fossil fuels.

- *Describe entry or sales barriers and how these are expected to be overcome.*

As mentioned in the risks associated with this project, there can be issues relating to the understanding of the product by end-users and furthermore, there is a global tendency to mostly consider battery-technologies, as the solution to achieving zero emission vehicles. Thus, a substantial job is required to inform, enlighten, and convince both policymakers, end-users, industries, etc., that other solutions and technologies exist.

We will try to change this public perception through demonstration, marketing, and publication of various findings in this project. Furthermore, collaboration with various vehicle manufacturers has been initiated going forward. The current attention to power-to-x activities helps these activities, as methanol is one of the proposed e-fuels available from such technologies.

The cost of fuel cell applications is another barrier to entry, however the reduction in waste-materials and optimization of internal processes, has decreased overall cost and a production scale-up will significantly reduce overall cost further. Thus, large scale implementation of fuel cell applications in e.g., vehicles, will be the main driver towards cost reductions.

- *How does the project results contribute to realise energy policy objectives?*

If implemented in the light commercial vehicle industry, the application in this project has the potential to reduce transport-emissions and pollution significantly, while maintaining performance from traditional internal combustion engine vehicles. Thus, this project's findings enhance the ability to achieve zero emission vehicles, in vehicles unfit for battery-applications, without compromising crucial performance objectives, necessary for the commercial vehicle industry.

This project has also achieved a significant rate of recyclability in materials previously not recycled. Furthermore, processes have been optimized to better utilize the materials, thereby reducing the amount of waste substantially, to a level compliant with circular economy principles.

- *If Ph.D.'s have been part of the project, it must be described how the results from the project are used in teaching and other dissemination activities.*

A Ph.D. project at DTU is established in connection to the CobraDrive project.

The Ph.D. candidate, Sanser Celenk, has been actively contributing to the university teaching in association with his research: These activities include:

-Assistance in teaching DTU course 47201: Engineering Thermodynamics (Spring 2020, 50 hours)

-Co-Supervising a special course student. Project title: Impedance spectroscopic study of HT-PEM fuel cell focusing on break-in process (Spring 2020, 50 hours)

-Assistance in teaching DTU course 47330: Energy Storage and Conversion (Autumn 2020, 100 hours)

-Co-Supervising a special course student. Project title: Fuel Cell Evaluation of Pt-alloy Catalysts Focusing on Performance and Degradation (Autumn 2020, 100 hours)

-Assistance in teaching DTU course 47201: Engineering Thermodynamics (Spring 2021, 50 hours)

-Assistance in teaching DTU course 47330: Energy Storage and Conversion (Autumn 2021, 100 hours)

-Co-Supervising a master thesis. Project title: Gas Diffusion Electrodes for HT-PEMFC (Spring-Autumn 2021, 200 hours)

In addition, the Ph.D. candidate has been in active dissemination including

Workshops

-Joint European Summer School on Fuel Cell, Electrolyser and Battery Technologies (JESS). (As a student) Athens, Greece. September 2020.

-Girls' Day in Science. (As a presenter) Technical University of Denmark, Kgs. Lyngby, Denmark. 6th of October 2021.

Manuscripts under preparation

-S. Celenk, S. M. Fernandez, L. N. Cleemann, Q. Li, J. O. Jensen. Combined effects of anode feed dilution and CO poisoning in high temperature PEM fuel cells with varying anode platinum loading. To be submitted to Applied Energy 2022.

-S. Celenk, J. O. Jensen, Q. Li, L. N. Cleemann. Systematic study of voltage cycling induced degradation in state of art high temperature PEM fuel cells. To be submitted to Journal of Power Sources, 2022.

-S. Celenk, J. O. Jensen, L. N. Cleemann, Q. Li. Time resolved degradation analysis of HT-PEFCs operating in range extender mode. To be submitted to Journal of Power Sources, 2022.

7. Project conclusion and perspective

- *State the conclusions made in the project. What are the next steps for the developed technology?*

The 5kW systems that were in focus in this particular project are not suitable for larger vehicles; it is however possible to join several 5kW units in order to provide the power needed to feed a large electric vehicle with renewable fuel cell energy. The next step is to look at order of magnitude scaling of the developed technologies, both at product level, stack level and production level. Thus, making it more feasible to introduce the technologies to mobility industries and other relevant stakeholders. Several collaborations on future projects, with various industry partners have been initiated, to demonstrate the capability of the application at a larger scale and get it to the market.

- *Put into perspective how the project results may influence future development*

The results of this project have illustrated the capabilities of fuel cell applications integrated in a vehicle, while simultaneously illustrating how material optimization and production scale-up can help drive down overall cost. Thus, the findings of the project will be publicised, marketed, lobbied, etc., to make sure that industries, policymakers, and the public, knows the potential of fuel cell applications and how it can help transition sectors into achieving CO₂-neutrality, while maintaining crucial performance characteristics of traditional vehicles.